NASA CONTRACTOR REPORT

A FEASIBILITY STUDY OF A MINIATURE SOLID-STATE PRESSURE TRANSDUCER

by C. D. Parker

Prepared by
RESEARCH TRIANGLE INSTITUTE
Research Triangle Park, N. C.
for Langley Research Center

NATIONAL AERONAUTICS AND SPACE ADMINISTRATION • WASHINGTON, D. C. • JULY 1969

NASA CR-1366

A FEASIBILITY STUDY OF A MINIATURE SOLID-STATE PRESSURE TRANSDUCER

By C. D. Parker

Prepared under Contract No. NAS 1-7489 by
RESEARCH TRIANGLE INSTITUTE
Research Triangle Park, N.C.

for Langley Research Center

NATIONAL AERONAUTICS AND SPACE ADMINISTRATION

For sale by the Clearinghouse for Federal Scientific and Technical Information
Springfield, Virginia 22151 – CFSTI price $3.00

FOREWORD

This report was prepared by the Research Triangle Institute, Research Triangle Park, North Carolina, on NASA Contract NAS1-7489, "A Feasibility Study of A Miniature Solid-State Pressure Transducer". This work was administered under the direction of the Flight Instrument Division, Langley Research Center, by Mr. Charles A. Hardesty.

This investigation was performed by the Engineering and Environmental Sciences Division of the Research Triangle Institute under the general direction of Dr. R. M. Burger. Dr. J. J. Wortman was Laboratory Supervisor and C. D. Parker was the Project Leader. Other Institute staff members contributing to this effort include T. E. Pardue, F. T. Wooten, P. P. Rasberry, R. T. Pickett, and H. L. Honbarrier. Special thanks are also due to Mr. Hardesty of Langley Research Center for many valuable suggestions and assistance in testing the transducers.

ABSTRACT

The piezojunction effect, i.e., the sensitivity of the electrical characteristics of a p-n junction to mechanical strain, is summarized and its potential as a stress transducing mechanism discussed. Several configurations are described which provide for using the piezojunction effect as the sensory phenomenon in a pressure transducer, including a unique silicon needle sensor with a p-n junction in the needle apex. Needle sensors with excellent electrical characteristics were fabricated and demonstrated to be extremely sensitive to stress. These were fabricated into pressure transducers which detected pressure differentials of less than 100 μHg.

CONTENTS

Section		Page
I	INTRODUCTION	1
II	THEORETICAL CONSIDERATIONS - A SUMMARY	3
	Energy Band Considerations	3
	Deformation Potential Coefficients	7
	Calculated Values of $\gamma_\nu(e)$	7
	Effect of Stress on p-n Junction Characteristics	13
III	PRESSURE TRANSDUCER CONFIGURATION	16
	The Silicon Needle Sensor Configuration	16
	The Simple Diaphragm	38
	The Indenter-Point Configuration	39
	Other Transducer Configurations	40
	Read-out Circuitry	42
IV	CONCLUSIONS AND RECOMMENDATIONS	45
APPENDIX A	THE RELATIONSHIP OF STRESS TO STRAIN	47
APPENDIX B	NEEDLE FABRICATION PROCEDURE	50
APPENDIX C	FUNDAMENTAL FREQUENCY OF A CIRCULAR DIAPHRAGM	57
REFERENCES		58

LIST OF ILLUSTRATIONS

Figure		Page
1.	The Valence Bands of Silicon Near $\bar{k} = 0$	4
2.	The Split Valence Bands of Silicon for a Compressional Stress	4
3.	Ratio of Stressed to Unstressed Minority Carrier Density for a Hydrostatic, [100], [011] and [111] Uniaxial, Compressional Stress	8
4.	Ratio of Stressed to Unstressed Minority Carrier Density for a [100], [011] and [111] Uniaxial, Tensional Stress	9
5.	Ratio of Stressed to Unstressed Minority Carrier Density for a [100], [011] and [111] Uniaxial, Compressional Stress	10
6.	Ratio of Stressed to Unstressed Minority Carrier Density for a [100], [011] and [111] Uniaxial, Tensional Stress	11
7.	Stressed and Unstressed V-I Characteristics of a p-n Junction (Silicon Needle Diode)	14
8.	Schematic of a Silicon Needle Sensor	17
9.	Photomicrograph of a Needle Sensor Prior to Metallization	17
10.	An Illustration of the Needle Sensor Transducer Configuration	18
11.	Oscillogram Illustrating the V-I-Stress Characteristics of a Needle Sensor (S#121)	19
12.	A Shadow-profile of a Needle Sensor (S#121)	20
13.	V-I Stress Characteristics of a Needle Sensor with Leaky Reverse Characteristics	21
14.	An Oscillogram of Frequently Observed Forward V-I Stress Characteristics	23
15.	A Shadow-profile Typical of the Sharpest Needle Sensors	23
16.	A Basic Pressure Transducer with a Clear, Quartz Diaphragm	24
17.	A Cut-a-Way View of a Pressure Transducer and Metal Housing	24
18.	A Photograph of a Complete Transducer and Housing	25
19.	Schematic of the Pressure Transducer Test Apparatus	26

LIST OF ILLUSTRATIONS (continued)

Figure		Page
20.	A Photograph of the Transducer Test Apparatus	27
21.	A Photograph of the Test Apparatus	27
22.	An Oscillogram of the Forward Characteristics of PT#14 with $\Delta P = 0$	28
23.	A Pressure Transducer Read-out Circuit (PT#14)	29
24.	Read-out Voltage vs. Differential Pressure, PT#14	30
25.	Low Pressure Characteristics of PT#14	31
26.	Forward V-I Characteristics of a Pressure Transducer (PT#9) with $\Delta P = 0$	32
27.	V-I-Stress Characteristics of a Needle Sensor (S#123)	32
28.	Read-out Voltage vs. Differential Pressure, PT#9	33
29.	V-I-Stress Characteristics of S#111	34
30.	Bridge Read-out Circuit for a Pressure Transducer	35
31.	Read-out Voltage vs. Differential Pressure, PT#8	36
32.	The Simple Diaphragm Pressure Transducer	38
33.	The Indenter-Point Pressure Transducer Configuration	39
34.	The Indenter-Point Transducer with Junction in Chip	40
35.	Output Voltage Pressure Characteristics of a Commercial Transducer Utilizing the Piezojunction Effect	41
36.	A Unijunction Oscillator Read-out Circuit	42
37.	A Diode-Resistor Bridge Read-out Circuit	43
38.	Output Voltage of the Diode-Resistor Bridge Circuit for $\Delta P = 0$ and $\Delta P = 10$ mm Hg	44
B-1.	A Photograph of the Needle Cleaning Fixture	53
B-2.	A Photomicrograph of a Group of Silicon Needles Illustrating the Uniformity that can be Achieved in Mechanical Shaping	53
B-3.	A Photographic Illustration of the Black-Wax Masking Procedure	56

n	electron density (cm^{-3})
n_o	electron density corresponding to zero stress (cm^{-3})
p	hole density (cm^{-3})
p_o	hole density corresponding to zero stress (cm^{-3})
q	electronic charge (1.602×10^{-19} C)
σ	stress level (dynes/cm^2)
σ_b	base-region stress (dynes/cm^2)
σ_e	emitter-region stress (dynes/cm^2)
T	absolute temperature (°K)
V	p-n junction voltage (V)
V_B	unstress breakdown voltage of a p-n junction (V)
Ξ_d	deformation potential coefficients
Ξ_u	deformation potential coefficients

A FEASIBILITY STUDY OF A MINIATURE SOLID-STATE PRESSURE TRANSDUCER

By C. D. Parker
Research Triangle Institute

SECTION I

INTRODUCTION

The objective of this study was to demonstrate the feasibility of using the piezojunction effect as the sensory phenomenon in a solid-state pressure transducer. The piezojunction effect, i.e., the sensitivity of the V-I characteristics of a p-n junction to stress, is an extremely sensitive mechanism and potentially provides for significant improvements in the transducer art. The piezojunction effect occurs at high stress levels ($\sigma > 10^9$ dynes/cm^2 in silicon) and is characterized by an exponential increase in minority carrier density as stress is increased above the threshold level. The minority carrier density is approximately linearly related to current in a forward biased p-n junction and an increase in the minority carrier density can be readily detected in the V-I characteristics of the junction. The exponential relationship between stress, minority carrier density and, consequently, forward current in a p-n junction make the piezojunction phenomenon particularly attractive as a stress transducing mechanism. Configurations which permit physical parameters such as pressure and acceleration to vary the stress applied to a p-n junction potentially provide for a family of sensitive piezojunction transducers.

This investigation was a continuation of a preceding feasibility study and largely builds on the results of that effort (Ref. 1). Prior to this investigation, the sensitivity of p-n junctions to stress had been demonstrated. The idea of a silicon needle sensor had been conceived as the solution to numerous problems associated with exploiting the piezojunction phenomenon and the feasibility of fabricating such a sensor demonstrated. Needle sensors had been fabricated into pressure transducers and used to detect changes in differential pressure. Several deficiencies in the needle sensor were obvious. Few were fabricated with desirable diode characteristics and contact to the diffused tip region depended upon a physical contact to that region. At the stress and current levels required for satisfactory performance, the physical contact is unreliable as an electrical contact. In order to eliminate the dependency on the physical contact between the needle tip and the material against which it is stressed (the diaphragm), several technical problems had to be solved. In particular, a double window masking process was

needed to provide positive isolation of the junction and a good passivating oxide was required to insulate the bulk silicon from the expanded aluminum contact.

Silicon needle sensors with desirable V-I-stress characteristics have been fabricated into sensitive pressure transducers which demonstrate the feasibility of exploiting the piezojunction effect as a stress transducing mechanism. The full potential of the piezojunction effect and especially of the silicon needle sensor, however, has not been demonstrated. Although processing procedures for fabricating silicon needle sensors evolved and were significantly refined, a sufficient number of sensors for carrying out the extensive experimental program needed in this effort could not be produced. The effects of changing physical characteristics of the silicon needle sensors such as principal axis orientation, bulk resistivity and needle-tip sharpness need to be experimentally evaluated, and a sufficient number of good quality sensors produced to provide for extensive parameter evaluation experiments in the pressure transducers. Pressure transducer parameters such as diaphragm size, thickness and material; bonding materials and over-pressure protective devices have not been adequately evaluated due to the shortage of sensors. A technology for fabricating needle sensors has evolved however, and the feasibility of a piezojunction pressure transducer demonstrated.

SECTION II

THEORETICAL CONSIDERATIONS - A SUMMARY

A complete theoretical discussion of the piezojunction phenomenon in silicon has been published by Wortman, et al., (Refs. 2-6). These discussions are summarized in this report in the interest of completeness.

Energy Band Considerations

The electrical characteristics of semiconductors and the piezojunction phenomenon are conveniently described in terms of the energy band structure. Silicon, as is the case for all semiconductors, has a forbidden energy region (energy gap) separating the valence energy levels (valence band) and the conduction energy levels (conduction band). In momentum space ($\bar{k}$-space), the maximum valence levels in silicon occur at $\bar{k}$ = (000) and the minimum conduction levels occur in the <100> directions.

The maximum valence levels, Γ'_{25}, have a separation resulting from the two angular momentum quantum numbers, j = 3/2 and j = 1/2. The j = 1/2 level is approximately 0.04 eV below the j = 3/2 level and is neglected in the computations that follow. The Γ'_{25} (j = 3/2) level is degenerate at $\bar{k}$ = (000) and is slightly split for $\bar{k} \neq$ (000) due to spin orbit coupling. The Γ'_{25} valence levels of silicon near k = (000) are illustrated for silicon in Fig. 1. The splitting of the Γ'_{25} (j = 3/2) level for $\bar{k} \neq$ (000) causes the effective masses for the two levels to be different, and the upper and lower levels are frequently referred to as "heavy" holes and "light" holes, respectively.

When stress is applied to the silicon crystal, the Γ'_{25} (j = 3/2) energy levels become non-degenerate as illustrated in Fig. 2. E_{V1} and E_{V2} are the Γ'_{25} (j = 3/2) "heavy" and "light" hole energy levels, and E_{V3} is the Γ'_{25} (j = 1/2) energy level. Since it is the width of the forbidden energy gap that is of interest, it is convenient to consider the change in the Γ'_{25} (j = 3/2) energy levels with strain. These are given by

$$\Delta E_{V1} = E_{V1} - E_o = D_d e + \{(\tfrac{2}{3} D_u)^2 (e_1^2 + e_2^2 + e_3^2 - e_1 e_2 - e_1 e_3 - e_2 e_3) + \tfrac{1}{3} (D'_u)^2 (e_4^2 + e_5^2 + e_6^2)\}^{1/2}, \quad (1)$$

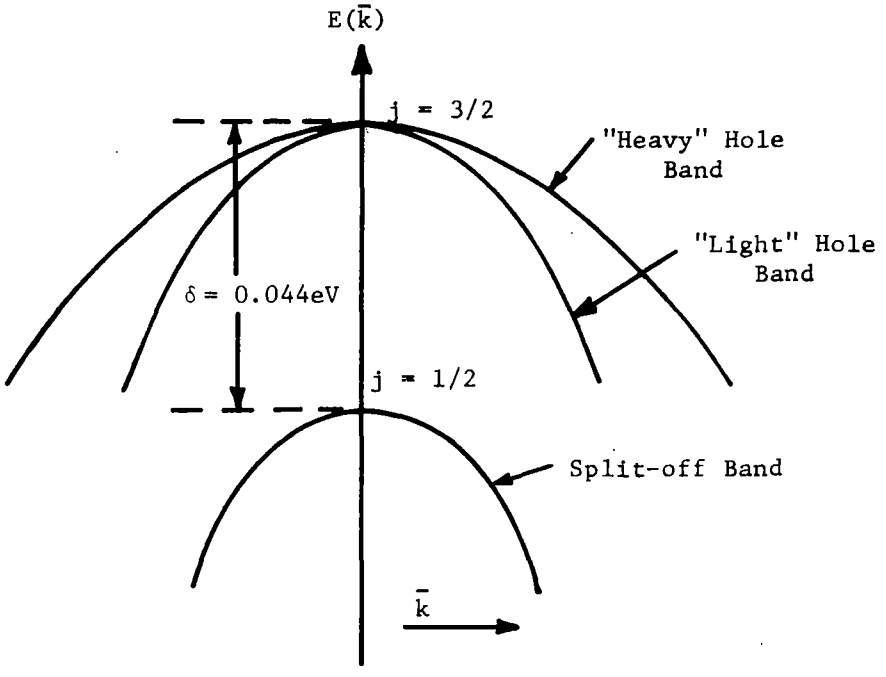

Figure 1. The Valence Bands of Silicon Near $\bar{k} = 0$ (Ref. 5)

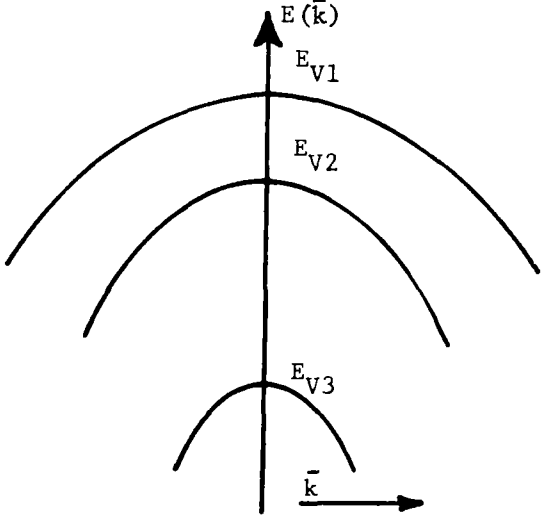

Figure 2. The Split Valence Bands of Silicon for a Compressional Stress (Ref. 5)

and

$$\Delta E_{V2} = E_{V2} - E_o = D_d e - \{(\frac{2}{3} D_u)^2 (e_1^2 + e_2^2 + e_3^2 - e_1 e_2 - e_1 e_3 - e_2 e_3) + \frac{1}{3} (D_u')^2 (e_4^2 + e_5^2 + e_6^2)\}^{1/2} , \quad (2)$$

where the D's are the deformation potential coefficients, the e_i's are the engineering strain components along the crystal axes (see Appendix A), and

$$e = e_1 + e_2 + e_3 . \quad (3)$$

More specifically, D_d is the energy level shift per unit dilation of the Γ_{25}' (j = 3/2) band edge, D_u is proportional to the splitting of the band edge induced by uniaxial shear strain along the [100] axis, and D_u' is proportional to the band edge splitting induced by uniaxial shear strain along the [111] axis. E_o is the unstrained Γ_{25}' (j = 3/2) energy level (Refs. 2, 5).

Strain also induces changes in the conduction bands, and changes in the conduction band minima are of equal importance with changes in the valence band maximum. Silicon has six conduction band minima located along the principal crystal axes. Since these minima change in pairs, i.e., since one cannot distinguish between the conduction band minima located along the [100] and [$\bar{1}$00] axes, only three conduction band minima need be considered, E_{C1}, E_{C2} and E_{C3}. Changes in these conduction band minima in the stress region of interest are given by (Refs. 2, 5)

$$\Delta E_{C1} = \Xi_d e + \Xi_u e_1 ,$$

$$\Delta E_{C2} = \Xi_d e + \Xi_u e_2 , \quad (4)$$

$$\Delta E_{C3} = \Xi_d e + \Xi_u e_3 ,$$

where the Ξ's are the deformation potential coefficients.

Changes in the valence band and conduction band maxima and minima energy levels gives rise to a change in the carrier concentrations in the conduction and valence bands. In silicon, for example, the density of electrons associated with the six conduction band minima is given by

$$n = 2\left(\frac{2\pi kT}{\hbar^2}\right)^{3/2} \{m_{C1}^{3/2} \exp[-(\frac{E_{C1} - E_F}{kT})] + m_{C2}^{3/2} \exp[-(\frac{E_{C2} - E_F}{kT})] + m_{C3}^{3/2} \exp[-(\frac{E_{C3} - E_F}{kT})]\} , \quad (5)$$

where E_F = the Fermi energy level, and

m_{Ci} = the effective electron masses associated with the energy minima. Under the application of stress, Eq. (5) can be written as

$$n = \frac{n_o}{3} \exp(\frac{\Delta E_F}{kT}) \left[\exp(-\frac{\Delta E_{C1}}{kT}) + \exp(-\frac{\Delta E_{C2}}{kT}) + \exp(-\frac{\Delta E_{C3}}{kT})\right] , \quad (6)$$

where n_o = unstressed electron density, and

ΔE_F = change in the Fermi energy.

Similarly, the carrier concentration associated with the valence band maxima is given by

$$p = 2\left(\frac{2\pi kT}{\hbar^2}\right)^{3/2} \{m_{V1}^{3/2} \exp[-(\frac{E_F - E_{V1}}{kT})] + m_{V2}^{3/2} \exp[-(\frac{E_F - E_{V2}}{kT})]\} \quad (7)$$

where m_{Vi} = effective masses associated with the valence band maxima (E_{Vi}). In Eq. (7), the Γ_{25}' (j = 1/2) energy level has been neglected. If the small difference between m_{V1} and m_{V2} is also neglected, a good approximation for silicon, Eq. (7) can be written for stressed conditions as

$$p = \frac{p_o}{2} \exp(-\frac{\Delta E_F}{kT}) \left[\exp(\frac{\Delta E_{V1}}{kT}) + \exp(\frac{\Delta E_{V2}}{kT})\right] , \quad (8)$$

where p_o = the hole concentration with no stress.

The $\exp(-\frac{\Delta E_F}{kT})$ terms in Eqs. (6) and (8) can be evaluated by setting the majority carrier density equal to the impurity density and assuming the ionization energy to be independent of stress. Consequently, the hole density remains constant in p-type material, for example, and

$$\exp(\frac{\Delta E_F}{kT}) = \frac{1}{2} \left[\exp(\frac{\Delta E_{V1}}{kT}) + \exp(\frac{\Delta E_{V2}}{kT})\right] . \quad (9)$$

Substituting Eq. (9) into (6) yields the ratio of stressed to unstressed minority carrier density, $\gamma_\nu(e)$, in the p-type material as (Ref. 2)

$$\gamma_\nu(e) = \frac{n_p}{n_{po}} = \frac{1}{6}\left[\exp\left(\frac{\Delta E_{V1}}{kT}\right) + \exp\left(\frac{\Delta E_{V2}}{kT}\right)\right]\left[\exp\left(-\frac{\Delta E_{C1}}{kT}\right) + \exp\left(-\frac{\Delta E_{C2}}{kT}\right) + \exp\left(-\frac{\Delta E_{C3}}{kT}\right)\right] . \tag{10}$$

Following a similar procedure for n-type material, it can be shown that (Ref. 2)

$$\frac{p_n}{p_{no}} = \frac{n_p}{n_{po}} = \gamma_\nu(e) . \tag{11}$$

Deformation Potential Coefficients

The deformation potential coefficients have been evaluated both theoretically and experimentally, and the values used herein are underlined in Table I. It is possible that the deformation potential coefficients change with doping. In particular, the value D_u' is considerably uncertain, and $\gamma_\nu(e)$ has been calculated using two different values of D_u'. The value of D_u' which should be used is not known; however, it is probably between 2.68 and 10. The value of 2.68 appears from experimental observations to be a better value.

Calculated Values of $\gamma_\nu(e)$

The ratio of stressed to unstressed minority carrier density, $\gamma_\nu(e)$, has been calculated for hydrostatic and uniaxial [100], [011] and [111] tensional and compressional stresses. Figures 3 and 4 are plots of $\gamma_\nu(e)$ as a function of compressional and tensional stresses, respectively, for $D_u' = 2.68$. Figures 5 and 6 are similar plots for $D_u' = 10$. For a hydrostatic and uniaxial [100] stress, $\gamma_\nu(e)$ is independent of D_u'. The exponential increase in $\gamma_\nu(e)$ with stress is a basic characteristic of the piezojunction phenomenon. It is evident from Figs. 3 - 6 that $\gamma_\nu(e)$ is most sensitive to a [100] compressional stress, and least sensitive to a [111] tensional stress. It is also evident that the piezojunction effect is significant at stress levels greater than 10^9 dynes/cm^2, i.e., order-of-magnitude changes occur in $\gamma_\nu(e)$ with changes in stress. The mechanical

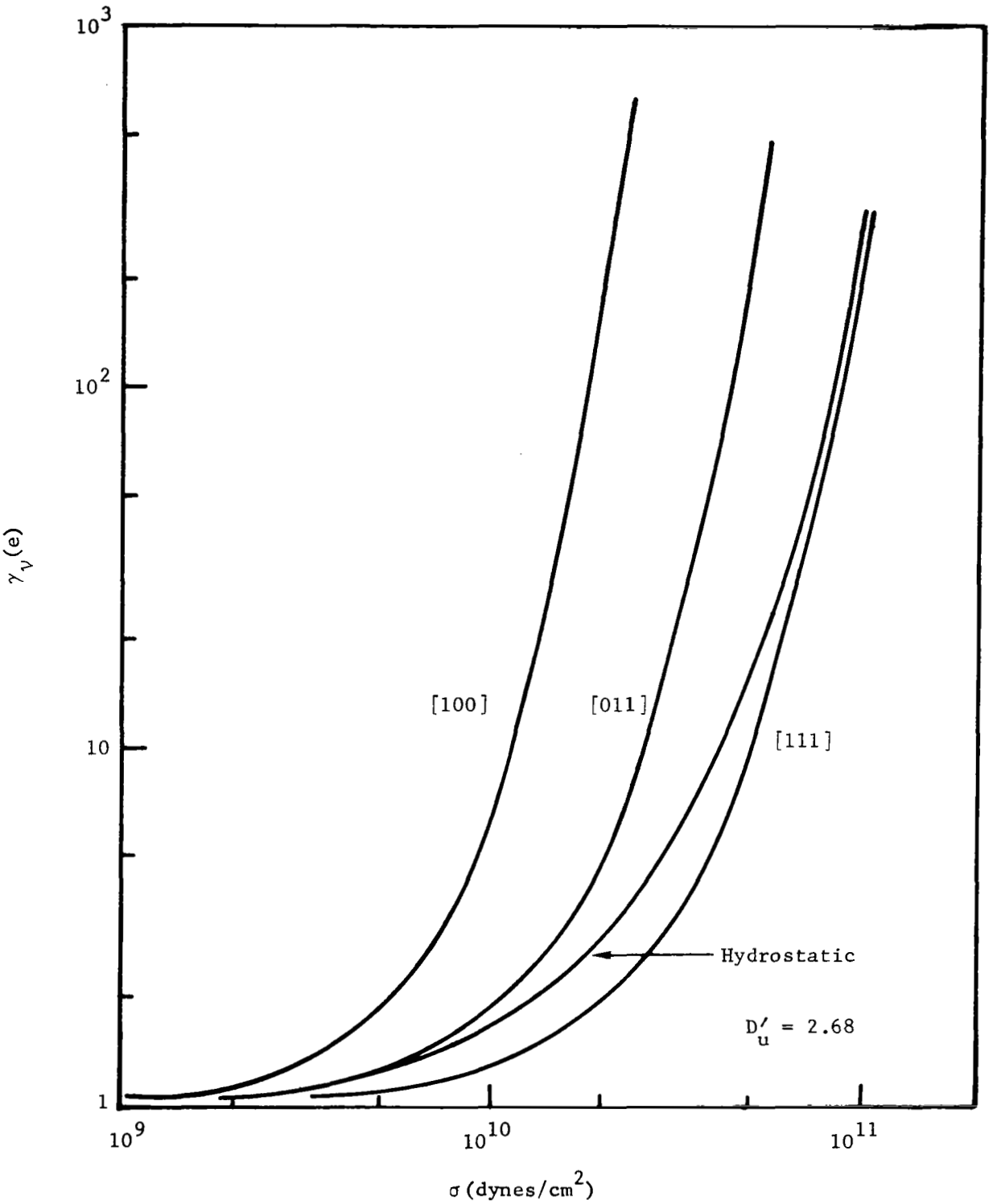

Figure 3. Ratio of Stressed to Unstressed Minority Carrier Density for a Hydrostatic, [100], [011] and [111] Uniaxial, Compressional Stress

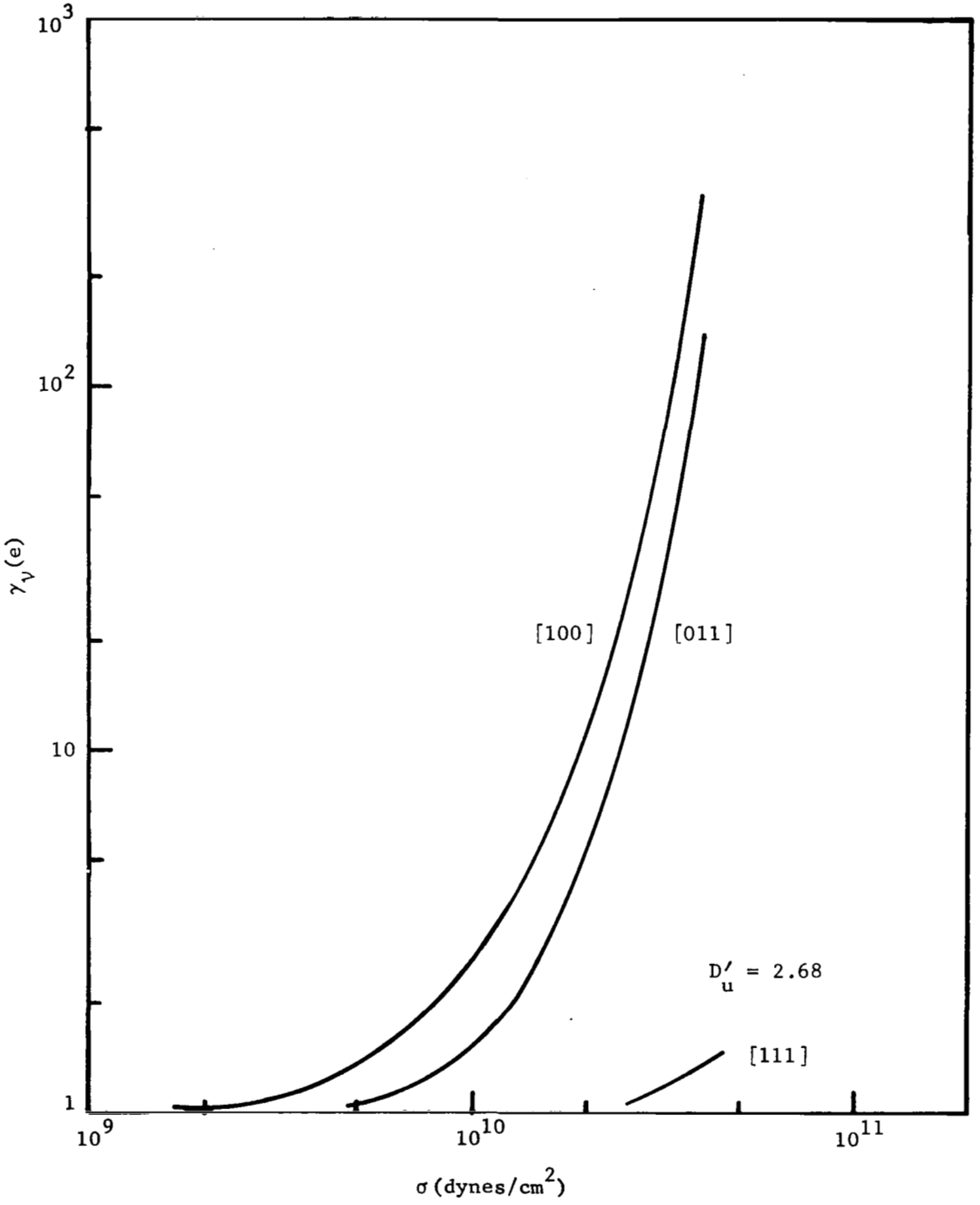

Figure 4. Ratio of Stressed to Unstressed Minority Carrier Density for a [100], [011] and [111] Uniaxial, Tensional Stress

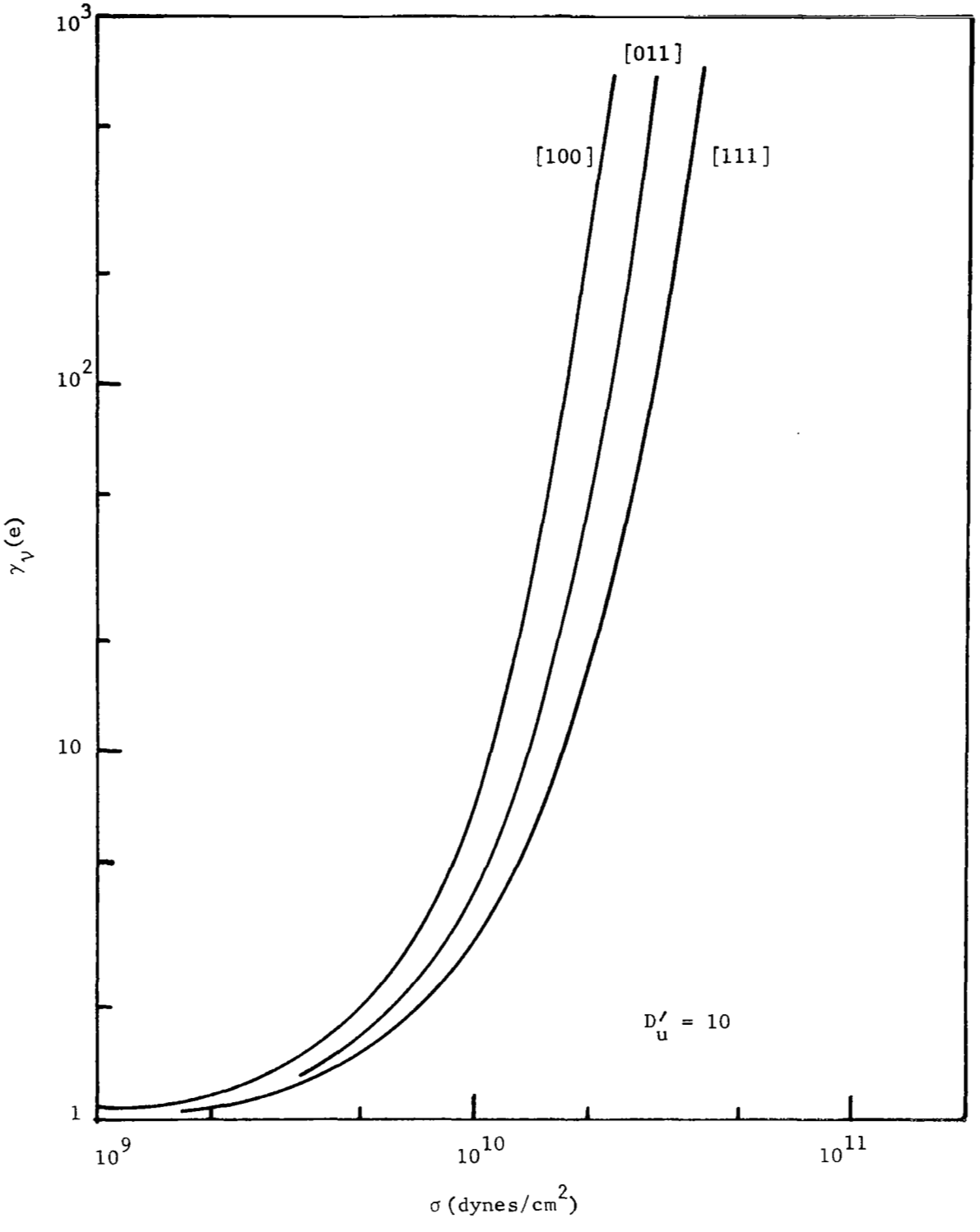

Figure 5. Ratio of Stressed to Unstressed Minority Carrier Density for a [100], [011] and [111] Uniaxial, Compressional Stress

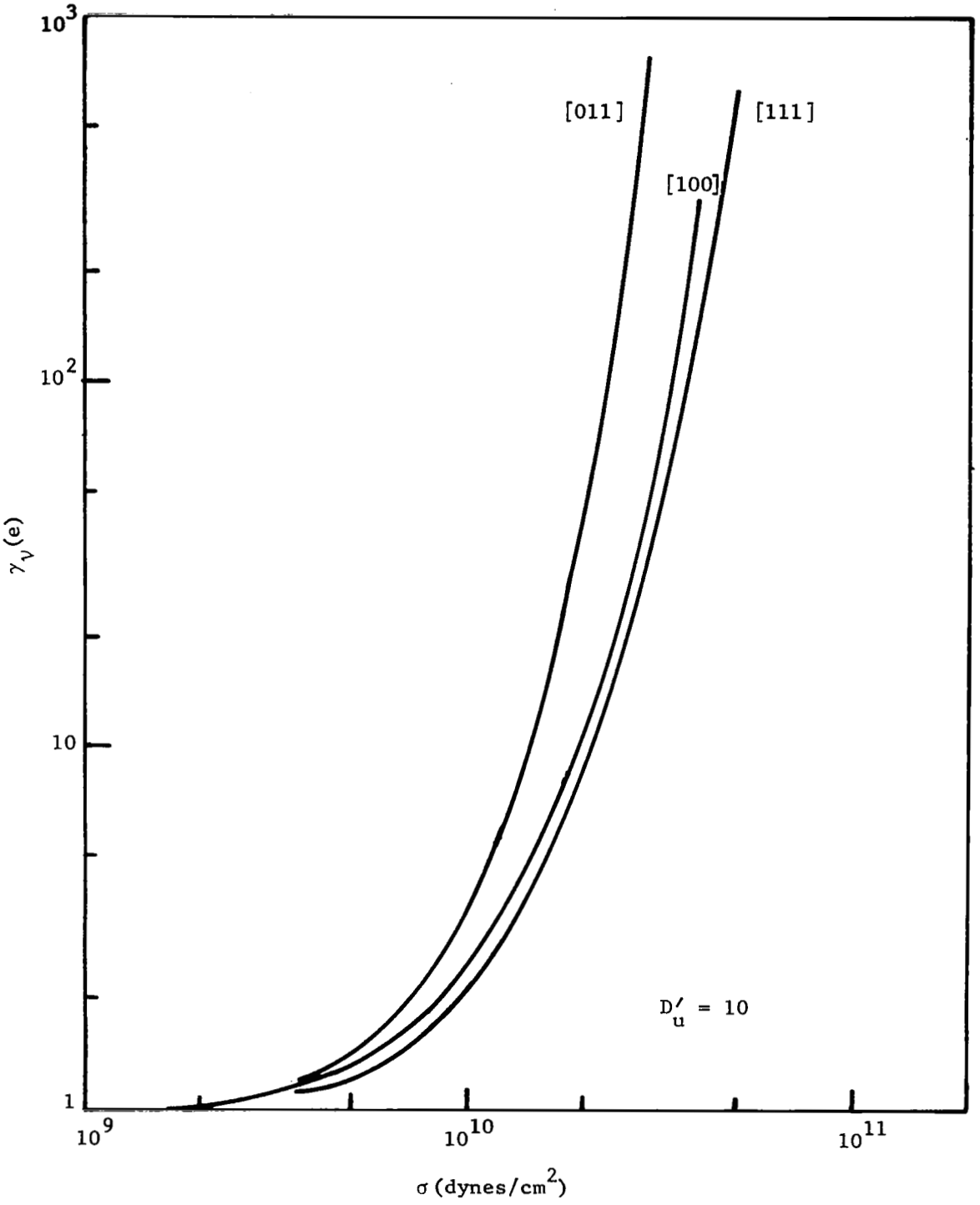

Figure 6. Ratio of Stressed to Unstressed Minority Carrier Density for a [100], [011] and [111] Uniaxial, Tensional Stress

Table I. (Ref. 4)

Deformation Potential Coefficients (eV/unit dilation) for Si. (Kleinman's Theoretical Values are Shown in Brackets. Values Used in This Investigation are Underlined.)

Coefficient	Si
D_d	[- 2.09]
D_u	2.04,[a] [3.74]
D_u'	2.68,[a] 10,[e] [4.23]
Ξ_d	[- 4.99]
Ξ_u	11,[b] 8.3,[c] [+ 9.6]
$D_d - (\Xi_d + \frac{1}{3}\Xi_u)$	- 1.44,[d] [- 0.30]

a J. C. Hensel and G. Feher, Phys. Rev. 129, 1041 (1963).

b D. K. Wilson and G. Feher, Phys. Rev. 124, 1968 (1961).

c J. E. Aubrey, W. Gubler, T. Henningsen, and S. H. Koenig, Phys. Rev. 130, 1667 (1963).

d W. Paul, J. Phys. Chem. Solids 8, 196 (1959).

e J. J. Wortman, Private Communication.

strength of silicon limits the stress that can be applied to a p-n junction in silicon and is the basic limitation to changes that can be achieved in $\gamma_\nu(e)$. The fracture strength of silicon varies from sample to sample and depends to a large extent on the surface conditions (Ref. 7). However, several order of magnitude changes have been experimentally observed in $\gamma_\nu(e)$.

Effect of Stress on p-n Junction Characteristics

The effect of stress on p-n junction characteristics has been described in terms of $\gamma_\nu(e)$ (Refs. 3, 5). Changes in other parameters are assumed to be negligible as compared with the exponential change of $\gamma_\nu(e)$ with stress above 10^9 dynes/cm^2. This model also neglects the contribution of surface generation-recombination currents.

The total current (I_T) in p-n junctions is the sum of the ideal current (I_T) and the generation-recombination currents (I_R).

$$I_T = I_I + I_R \ . \tag{12}$$

For forward biased conditions, the bulk generation-recombination current is given approximately by (Ref. 3)

$$I_R = \frac{a\ \gamma_\nu(e)\ [\exp(qV/kT)-1]}{1 + b\ \sqrt{\gamma_\nu(e)}\ \exp(qV/kT)} \ , \tag{13}$$

and the ideal current is given by

$$I_I = c\ \gamma_\nu(e)\ [\exp(qV/kT)-1] \ , \tag{14}$$

such that Eq. (12) becomes (Ref. 3)

$$I_T = \frac{a\ \gamma_\nu(e)\ [\exp(qV/kT)-1]}{1 + b\sqrt{\gamma_\nu(e)}\ \exp(qV/2kT)} + c\ \gamma_\nu(e)\ [\exp(qV/kT)-1] \ . \tag{15}$$

The effect of stressing only part of the total junction area is accounted for by considering that the total diode consists of two diodes in parallel, i.e., (1) a stressed diode, and (2) an unstressed diode. If the total area is A, for example, and the stressed area is A_s, then Eq. (14) becomes (Ref. 3)

$$I_I = \left[\frac{(A - A_s)}{A} + \frac{A_s}{A}\ \gamma_\nu(e)\right]\ [\exp(qV/kT)-1] \ . \tag{16}$$

It is of interest here to consider the p-n junction current under different bias conditions. For large forward biases, Eq. (15) is approximately

$$I_T \simeq \frac{a}{b}\ (\gamma_\nu(e))^{1/2}\ \exp(qV/2kT) + c\ \gamma_\nu(e)\ \exp(qV/kT) \ . \tag{17}$$

It is significant that for large forward biases, i.e., V > 0.3 volts, p-n junction current will have a larger dependence on the ideal component of current than the generation-recombination component. In experiments with mesa diodes, the forward-bias characteristics have been dominated by the generation-recombination (qV/2kT) current at voltages less than a few tenths of a volt, and by the ideal (qV/kT) current at higher voltages. For reverse-bias conditions the ideal current is much less than the generation-recombination current. The effects of stress on the generation-recombination current in the reverse-biased mode is not easily described. Experimentally, reverse-biased p-n junctions have been observed to be very sensitive to stress and relatively independent of voltage for voltages less than the breakdown voltage. The forward-biased characteristics, as shown in Eq. (17), is dependent upon $\gamma_v(e)$ and the applied voltage. Both stressed and unstressed p-n junction V-I characteristics are illustrated in the oscillogram of Fig. 7. This junction was formed at the apex of a silicon needle.

Hauser and Wortman (Ref. 4) have also investigated the effect of mechanical stress on the breakdown voltage of p-n junctions and, in the case of silicon, found the change in breakdown voltage to be

$$\frac{\Delta V}{V_B} \approx - (10^{-12}\ \text{cm}^2/\text{dyne})\ \sigma \qquad (18)$$

where σ is the applied stress, ΔV is the change in breakdown voltage and V_B is the unstressed breakdown voltage. The change in breakdown

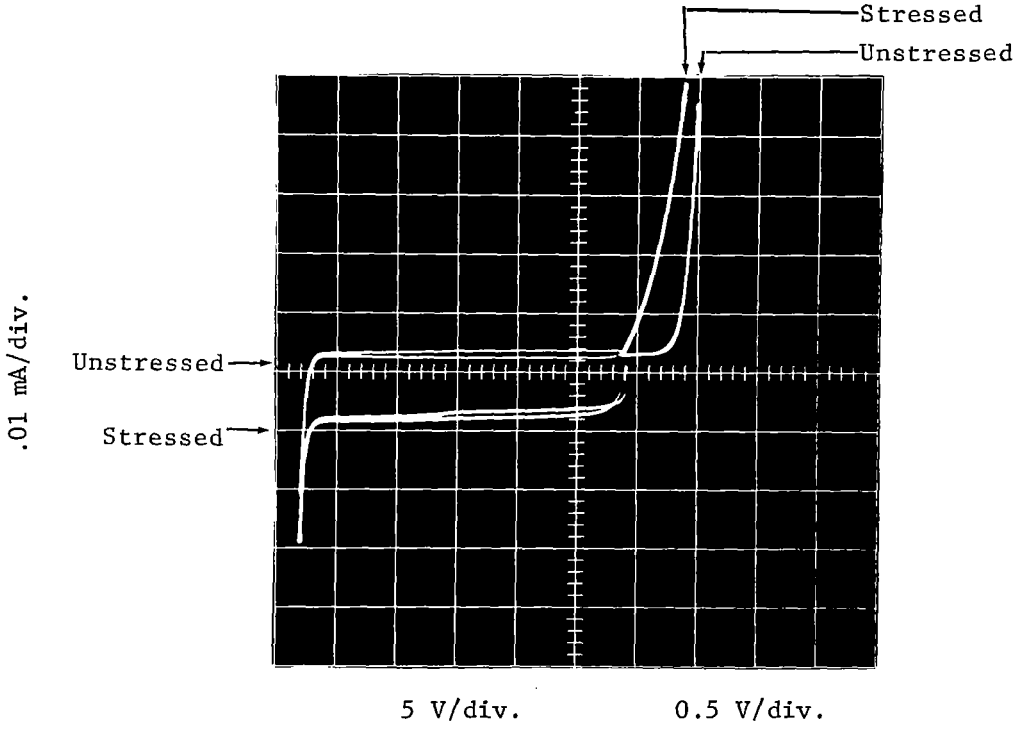

Fig. 7. Stressed and Unstressed V-I Characteristics of a p-n Junction (Silicon Needle Diode)

voltage is also independent of orientation. Since the breakdown voltage is a linear function of stress whereas junction current is an exponential function of stress, the latter mode of operation is potentially a more sensitive transducing mechanism. However, breakdown voltage is less sensitive to temperature changes than junction currents, and this mode of operation may have advantages in some applications.

The effects of stress on more complex silicon p-n junction structures is also of interest. Investigations of the effects of stress upon transistor characteristics and p-n-p-n switches have been performed (Ref. 2). If both sides of the emitter-base junction are stressed, the base and collector currents are changed several orders of magnitude for small changes in stress above the threshold value, and current gain is not affected. If only the emitter side of the junction is stressed ($\sigma_e >> \sigma_b$) the base current increases orders of magnitude with stress while the collector current remains unchanged. Consequently, gain is reduced by stressing the emitter side of the base-emitter junction. If only the base side of the junction is stressed ($\sigma_e << \sigma_b$), the base and collector currents remain approximately the same.

The effect of stress on p-n-p-n diodes has also been investigated and concluded to be a complex function of numerous variables, e.g., the uniformity and location of the applied stress. The switching voltage can increase or decrease with an increasing stress depending upon these various factors. The changes in switching voltage with stress can be very large, however, and the four-layer configuration is a promising transducer configuration.

SECTION III

PRESSURE TRANSDUCER CONFIGURATION

In order to utilize the stress sensitivity of a p-n junction as the sensory phenomenon in a pressure transducer, a transducer configuration is required in which pressure variations cause a variance in the stress applied to the junction. Of the various transducer configurations which have been considered, the silicon needle sensor is concluded to be the most advantageous. The concept of the needle sensor evolved as a solution to several problems associated with exploiting the piezojunction phenomenon in transducers. Conceptually, there are no limitations to the quality of a p-n junction fabricated in the needle configuration, the junction area can be made small and alignment problems are non-existent. The fundamental disadvantages of the needle sensor are also characteristic of every other workable configuration.

The Silicon Needle Sensor Configuration

The silicon needle sensor is illustrated schematically in Fig. 8, and a typical sensor is shown in the photomicrograph of Fig. 9. The p-n junction is fabricated in the needle tip by adapting planar processing technology to the needle configuration. Typically, the bulk silicon is 1 Ω-cm, n-type; the radius of curvature at the tip is 1 mil; the shank is 40 mils; and the junction depth is 2 microns. A double-window process is used to open diffusion and contact windows, and an expanded aluminum contact is utilized to contact the p-type region. The photomicrograph of Fig. 9 was taken prior to the aluminum metallization step and diffusion and contact windows are clearly visible. A procedure for fabricating silicon needle sensors is described in Appendix B.

The basic structure of the needle sensor transducer configuration is illustrated in Fig. 10. A rigid housing positions the needle sensor firmly against the diaphragm. Differential pressure variations across the diaphragm vary the stress applied to the needle sensor by the diaphragm and cause the V-I characteristics of the sensor to change.

Needle sensor fabrication and results. - As the difficulties associated with fabricating the silicon needle sensors were solved, a significant yield of sensors was achieved. After the initial successes, the process continued to evolve to the process described in Appendix B which yielded the best results. Numerous variations on this process were used with equal success. Any variations must be compatible with semiconductor processing techniques and, as always, cleanliness is essential. The critical steps appeared to be the mechanical shaping and the masking steps. Mechanical shaping is probably critical because it determines the condition of the silicon surface. The process described in Appendix B is not an optimum

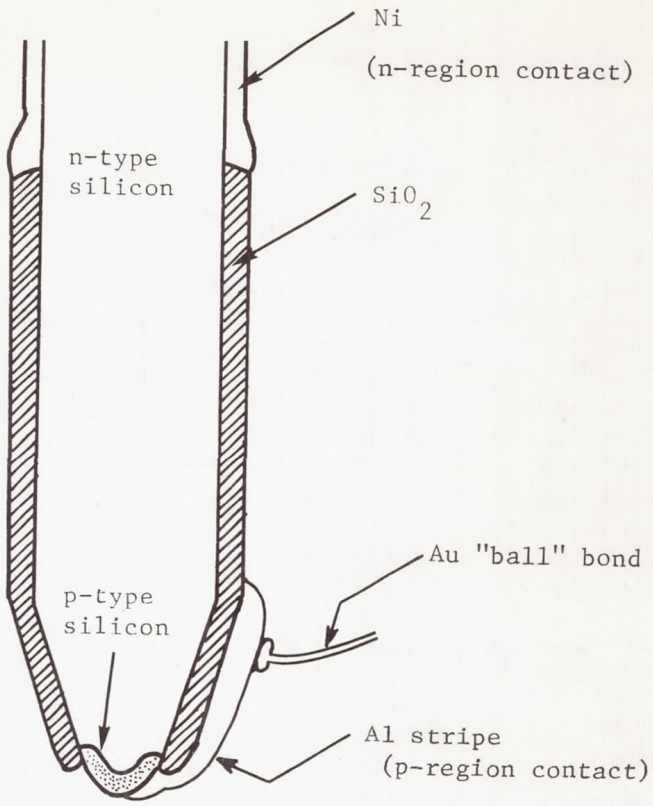

Figure 8. Schematic of a Silicon Needle Sensor

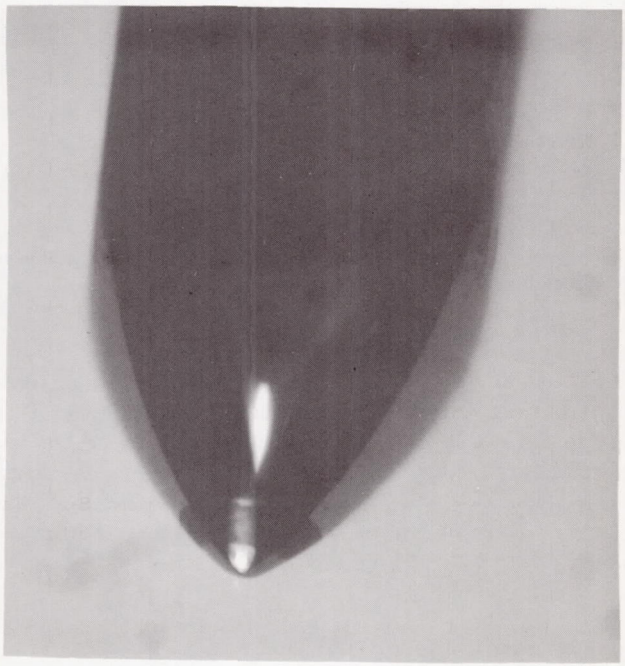

Figure 9. Photomicrograph of a Needle Sensor Prior to Metallization

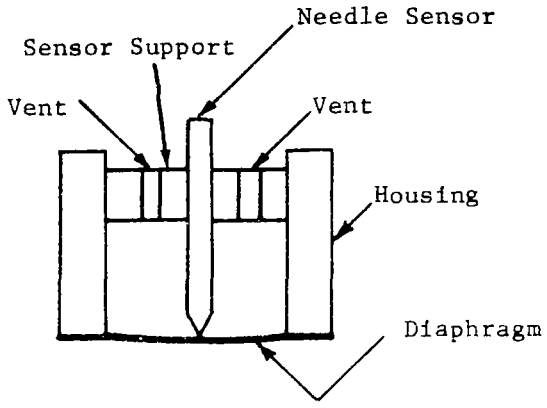

Figure 10. An Illustration of the Needle Sensor Transducer Configuration

process but one that yielded consistently good results. It is probable that further improvements are needed in order to realize the full potential of silicon needle sensors. Some of the best of the needle sensors are described in the following paragraphs and figures.

A unit with excellent V-I characteristics is illustrated in the oscillograms of Fig. 11. In the forward characteristics, the three curves correspond to zero force against the tip of the needle, a 15g force and 25g force. (The gram forces are approximate, e.g., $\pm$ 10 percent). Changes in the V-I characteristics of this sensor as the force is increased tend to be ideal, i.e., the characteristics move horizontally across the scope. The reverse characteristics also correspond to zero, 15g and 25g forces. The zero stress curve shows the sensor to be an excellent diode. Generally the reverse characteristics tend to be more leaky. This sensor (S#121) was eventually fabricated into a pressure transducer (PT#14) with excellent results.

A shadow profile of S#121 is shown in the photomicrograph of Fig. 12. Successive 90° rotations of the sensor showed an identical profile. The radius of curvature on the tip is approximately 0.5 mils and the included solid angle approximately 90°. The solid angle was eventually standardized to 60° although units with angles less than 45° were successfully processed. Efforts to increase the sharpness of the tip, i.e., reduce the radius of curvature, were not completely successful.

Forward

Vertical: 0.01 mA/div.
Horizontal: 0.1 V/div.
F = 0
≃ 15g
≃ 25g

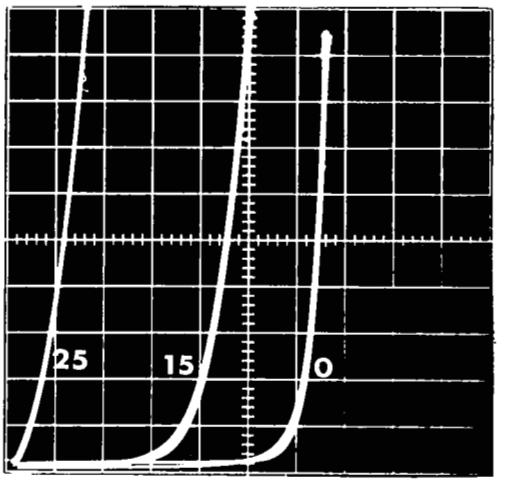

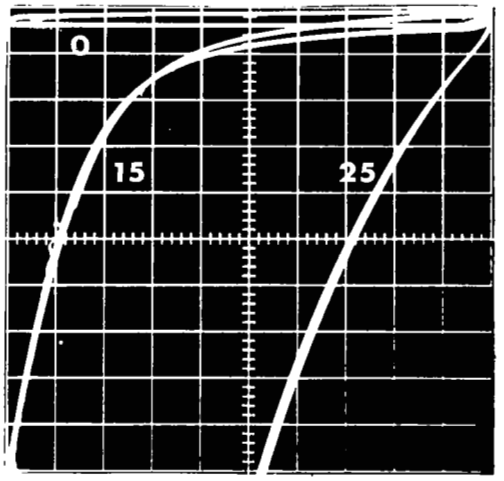

Reverse

Vertical: 0.01 mA/div.
Horizontal: 1.0 V/div.
F = 0
≃ 15g
≃ 25g

Figure 11. Oscillogram Illustrating the V-I-Stress Characteristics of a Needle Sensor (S#121)

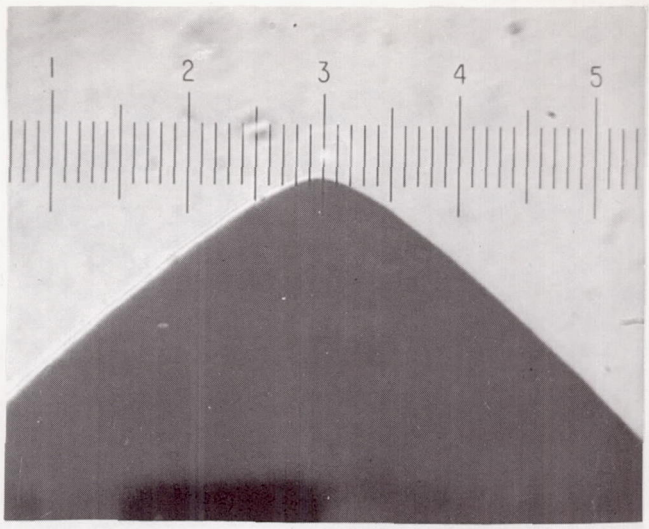

Figure 12. A Shadow-profile of a Needle Sensor (S#121). (Scale: 0.005 mm/div.; ≃ 0.197 mils/div.)

The reverse characteristics of S#121 tended to be the exception rather than the rule although several units were fabricated with these characteristics. More frequently, the reverse characteristics tended to be leaky, noisy and less stable. The sensor illustrated in Fig. 13 (S#153) is typical of most of the sensors fabricated, i.e., the forward characteristics were excellent and the reverse characteristics poor. The characteristics in Fig. 13 correspond to a zero force and a 30g force applied to the tip of the needle.

Two other variations in the experimental results are notable. In some instances the change in forward V-I characteristics with applied stress was not a horizontal shift as illustrated in Figs. 11 and 13. A frequently observed characteristic is illustrated in Fig. 14 (S#125) in which the slope of the forward characteristic changes significantly at any fixed current level as stress is increased. These units usually had a less-than-expected forward breakover voltage, e.g., less than 0.6 volts. Generally, these sensors were less sensitive to stress than the ideal units and were not fabricated into pressure transducers.

The reverse characteristics illustrated in Fig. 7 were also unusual. Such units tended to be less sensitive in both forward and reverse directions, but at some relatively high force level the reverse characteristics would vary as illustrated. These sensors tended to be unstable in that they suddenly changed to become a relatively insensitive version of the reverse characteristics illustrated in Fig. 14. All of these sensors were physically similar to the sensor shown in Fig. 9.

Forward

Vertical: 0.01 mA/div.
Horizontal: 0.1 V/div.
F = 0
≃ 30g

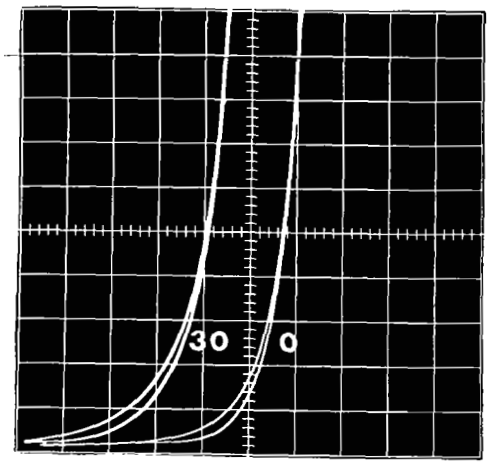

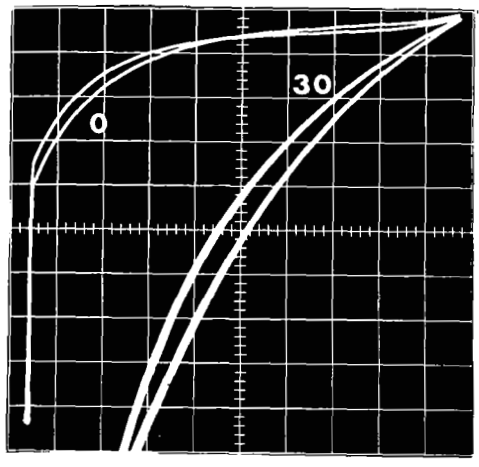

Reverse

Vertical: 0.01 mA/div.
Horizontal: 1.0 V/div..
F = 0
≃ 30g

Figure 13. V-I Stress Characteristics of a Needle Sensor with Leaky Reverse Characteristics

An obvious approach to increasing the sensitivity achieved with ideal sensors such as S#121 was to increase the sharpness of the sensor itself. The mechanical shaping process was modified to yield sharper points such as those illustrated in Fig. 15. In this case, the radius of curvature is 0.2 mils and the included solid angle is 30°. These units were readily fabricated through the mechanical shaping steps, but the processed sensors were unsatisfactory. Optical examination of these sensors showed clearly defined diffusion and contact windows, and no apparent reason for the lack of success. Time permitted only a limited number of these sharper needles to be processed and it is probably that a continued effort would eventually be successful.

Pressure transducer fabrication. - Most of the transducers fabricated during this study were basically as illustrated in Fig. 10. Figure 16 is a photograph of a basic transducer looking through the clear, quartz diaphragm into the sensor-side pressure port. Four vents are in evidence, and the sensor extends through a center hole to the rear of the transducer. Epoxy bonds are used throughout the unit. Pressure variations across the quartz diaphragm vary the stress on the sensor. All of the transducers to be described are similar to this illustration. The needle sensors have been improved and their shapes altered, physical dimensions have been changed and diaphragm materials have changed. The assembly of a transducer such as illustrated in Fig. 16 is basically as follows: the housing is completely assembled except for the needle sensor, and supported by placing the diaphragm face-down on a short piece of tubing similar to the tubing used to fabricate the housing. The needle sensor is held by a pin-vice in a micro-manipulator, positioned over the center hole and lowered so the sensor tip is inside the center hole. Epoxy is applied to the sensor shank and the sensor is lowered until the tip contacts the diaphragm and is suitably stressed. Everything is held rigidly until the epoxy bond between the sensor and housing cures. The V-I characteristics of the sensor are monitored with a curve tracer throughout the assembly. The gold wire bonded to the expanded aluminum contact to the p-region is fed through the center hole with the sensor and is accessible at the back of the housing.

An earlier practice was to fill an enlarged center hole with epoxy and drill a hole in the epoxy for the sensor. This practice proved to be unnecessary. The transducer shown in Fig. 16 was assembled this way.

The basic transducer illustrated in Figs. 10 and 16 was enclosed in a metal housing to facilitate handling and laboratory testing. The completed transducer is shown schematically in the cut-a-way drawing of Fig. 17. Test apparatus was designed to be compatible with this housing and it was used for most transducers. A conductive silver paste, DuPont type 6730, was used to connect gold wires to the back of the sensor shank and the metal feed-through ports. The end fittings on the housing are stock items. A photograph of a completed transducer is shown in Fig. 18.

Vertical: 0.01 mA/div.
Horizontal: 0.05 V/div.

F = 0
≃ 20g
≃ 30g

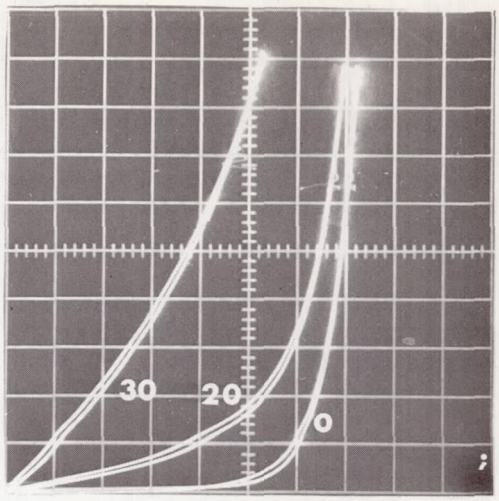

Figure 14. An Oscillogram of Frequently Observed Forward V-I Stress Characteristics

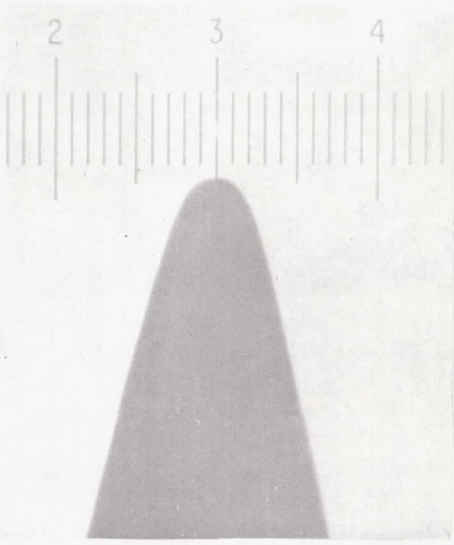

Figure 15. A Shadow-profile Typical of the Sharpest Needle Sensors (Scale: 0.0025 mm/div.)

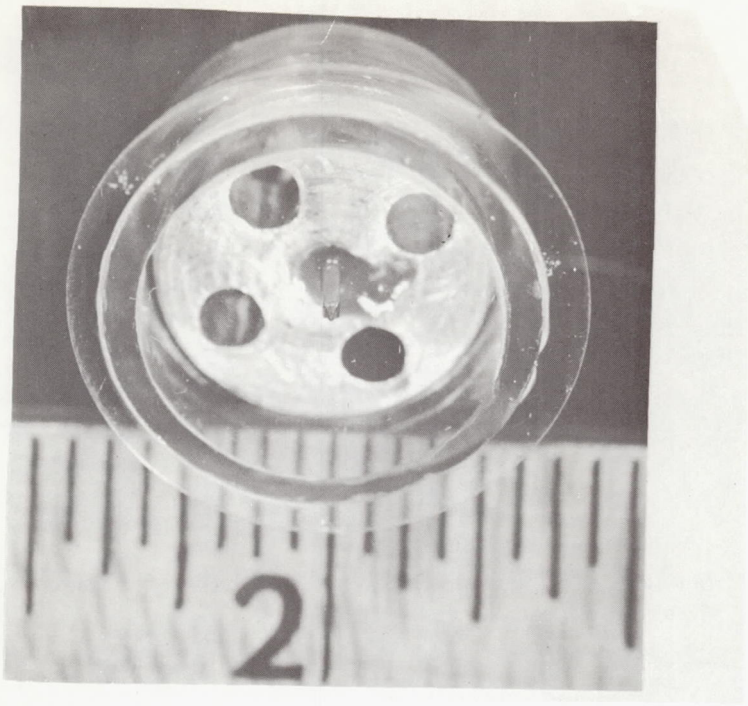

Figure 16. A Basic Pressure Transducer with a Clear, Quartz Diaphragm

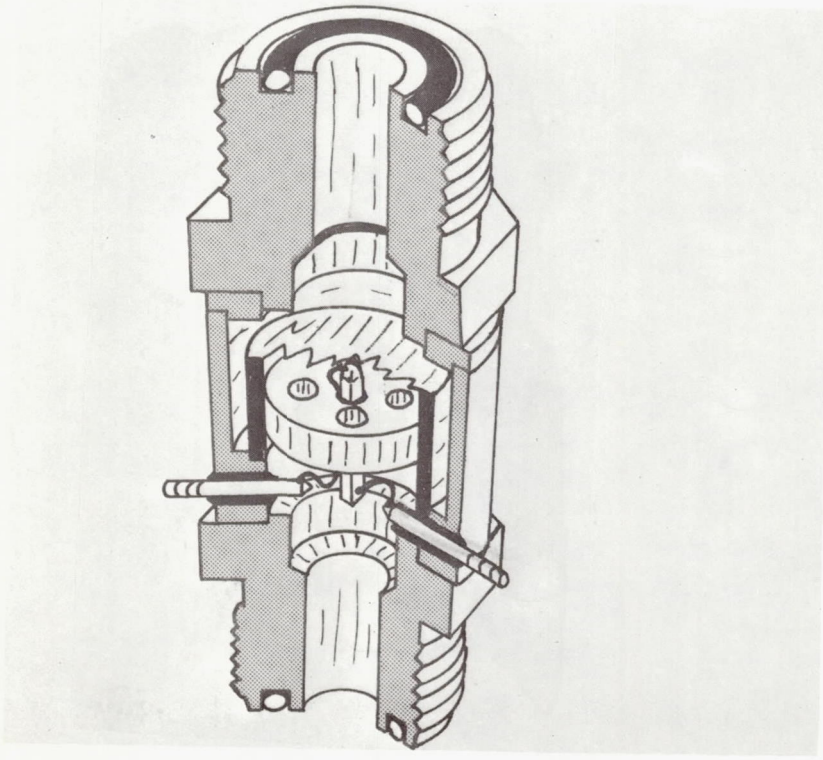

Figure 17. A Cut-a-Way View of a Pressure Transducer and Metal Housing

Figure 18. A Photograph of a Complete Transducer and Housing

A partially complete housing also proved to be a convenience during transducer fabrication. By completing the transducer except for the sensor and end fitting on the sensor side of the diaphragm, the sensor could be positioned essentially as described previously with an added convenience. A pressure or a vacuum could be used on the diaphragm side of the unit to enhance the positioning of the sensor. This procedure was employed in an effort to assemble an absolute transducer. It can also be used to counter a tendency for stress on the sensor to be relieved during assembly that was evident in the assembly procedure described previously.

Experimental results. - Experimental test data from several of the pressure transducers are presented and discussed in this section. All of the units described were fabricated in the standard configuration described in the preceding section. Attention is called to any variations in the mechanical characteristics or fabrication techniques that exist.

The transducer test apparatus is illustrated schematically in Fig. 19 and photographically in Figs. 20 and 21. Figure 20 is an overall view of the test apparatus showing the vacuum system and test instrumentation. (The transducer mounted in the bell jar does not have the standard housing.) Figure 21 is a view from the underside of the bell jar showing the plumbing, valve number 1 in Fig. 19, and the standard transducer (partially hidden by the support post). The bell jar enclosure is part of a laboratory vacuum system with a 4 inch diffusion

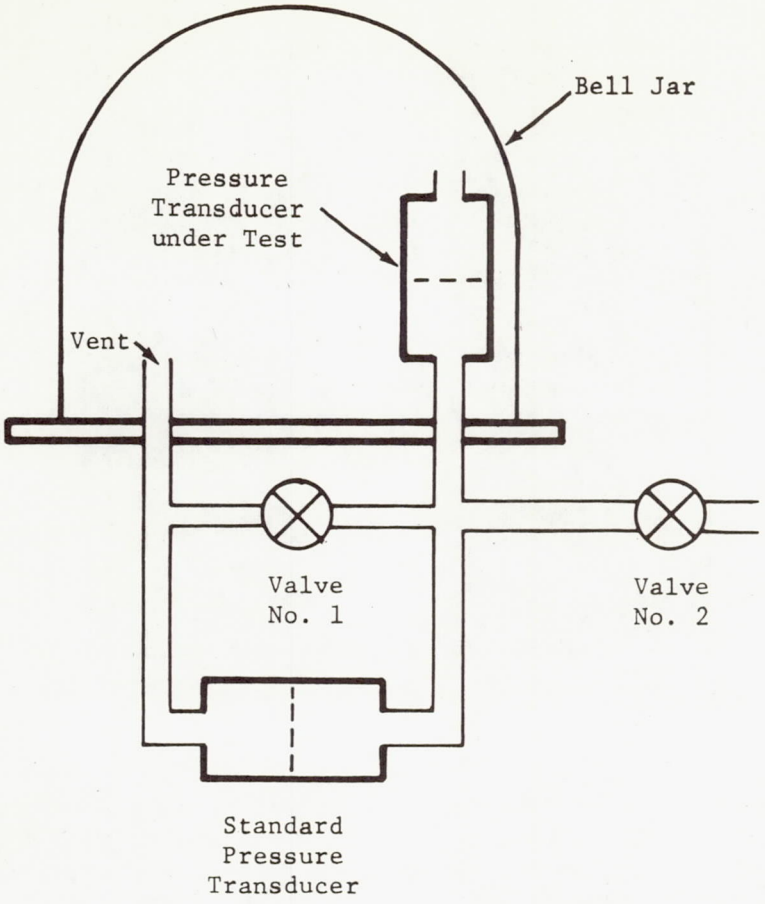

Figure 19. Schematic of the Pressure Transducer Test Apparatus

pump backed by a two-stage mechanical pump. The low pressure side of both the transducer under test and the standard transducer are ported together in the bell jar and the high pressure sides are ported together by 3/8" copper tubing. The high pressure sides and low pressure sides of the transducers can be ported together or isolated by opening or closing valve number 1. The usual test procedure is to close valve number 2, open valve number 1 and pump the entire system down to a low pressure, e.g., 10^{-5} mm Hg. With the entire system at low pressure, valve number 1 is closed isolating the low and high pressure sides of the transducers, and valve number 2 is used to control the differential pressure. After the differential pressure has been increased, it can be reduced again by closing valve number 1 and permitting a controlled leak through valve number 2. This system and procedure provided adequate control of static pressure across the transducers.

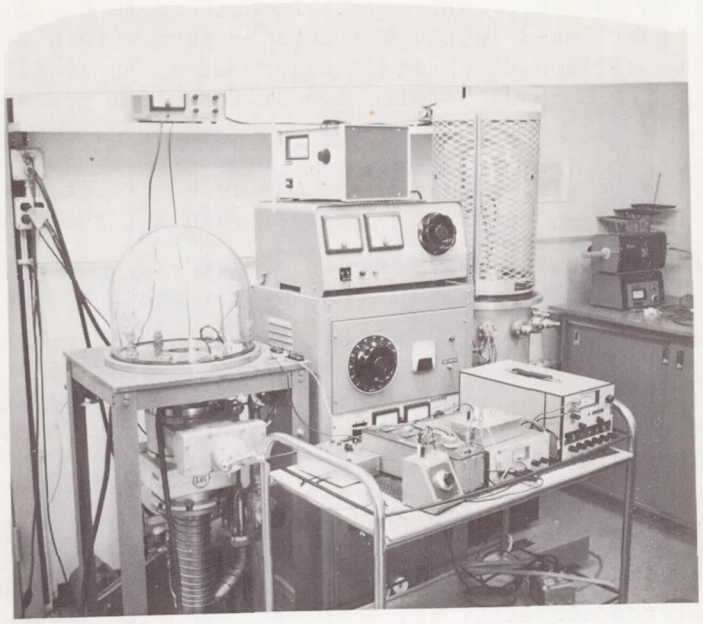

Figure 20. A Photograph of the Transducer Test Apparatus

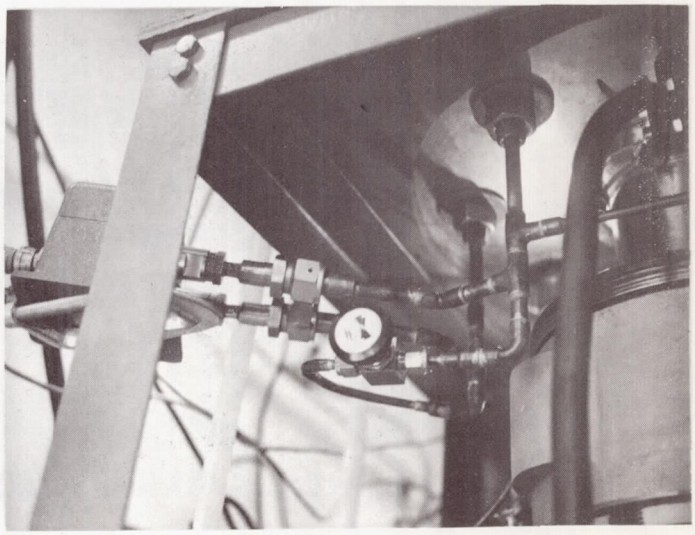

Figure 21. A Photograph of the Test Apparatus

The best experimental results were achieved with a pressure transducer (PT#14) fabricated with a needle sensor described in a preceding section, S#121. The V-I-stress characteristics of this sensor are shown in Fig. 11. This transducer was fabricated in the standard housing with a 2.5 mil thick and 7 mm radius silicon diaphragm. Figure 22 is an oscillogram of the forward characteristic of PT#14 with the differential pressure zero ($\Delta P = 0$).

The circuit shown in Fig. 23 was used as a test circuit for this transducer. Since R_1 was a factor of 20 larger than R_4, the presence of the amplifier in this circuitry had a negligible effect on the transducer and R_4. An effort was made to make R_4 small with respect to the forward impedance of the transducer so that the voltage across the transducer would remain relatively constant. An optimum forward bias of 0.35 volts was selected for the transducer experimentally. The potentiometer was adjusted so that when the differential pressure was zero the amplifier output was zero. The gain of the amplifier was 100.

The initial performance of this transducer is illustrated in Figs. 24 and 25. As illustrated in Fig. 24, a significant spread in the data occurred for pressure differentials below 0.3 mm Hg. At higher pressures, excellent repeatability was achieved. In Fig. 25, actual data points are included to illustrate the character of the data spread. The solid figures in Fig. 25 were recorded as ΔP was increased and the open figures as ΔP was reduced. These data were recorded over a period of several days. In each case, the differential pressure was caused to

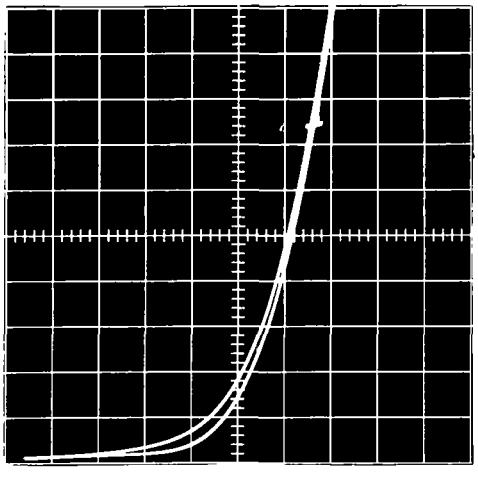

Vertical: 0.01 mA/div.
Horizontal: 0.05 V/div.

Figure 22. An Oscillogram of the Forward Characteristics of PT#14 with $\Delta P = 0$

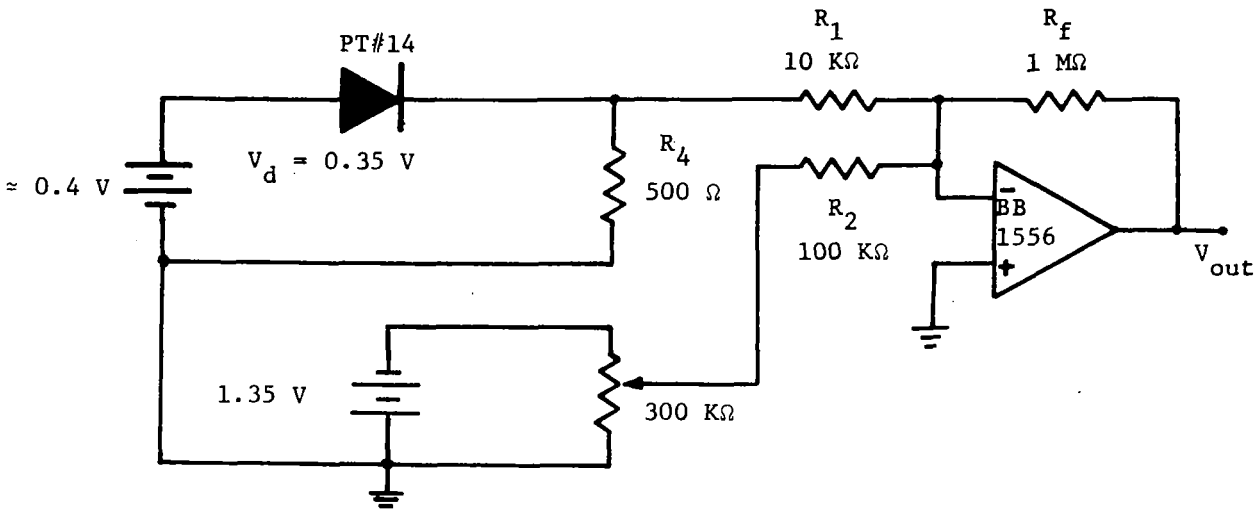

Figure 23. A Pressure Transducer Read-out Circuit (PT#14)

increase from zero to 10 mm Hg and return. If the differential pressure was limited to a lower value the data spread tended to be reduced also. It is significant to note that the output voltage on a given run did not consistently return by way of a higher or lower output voltage. This was not generally true of all transducers tested. All of these data were recorded at room temperature. The dotted lines in Fig. 25 correspond to $\pm$ 30 percent of reading error bands from the drawn-in straight line.

Several factors are notable about PT#14. First, the silicon needle sensor used in its fabrication was excellent. Secondly, its initial stress bias, i.e., the stress corresponding to $\Delta P = 0$, was relatively low. Neither of these factors are unique, however. Finally the V-I characteristics of this transducer did change significantly under storage conditions. The change appeared as a reduced stress possibly implying a creep in the housing components. After storage the transducer was accidentally damaged before additional data could be taken.

A short-term drift could be observed in the output of the read-out circuitry with $\Delta P = 0$. The drift was not monodirectional. The magnitude of the drift was appreciable as compared to the variations in the read-out at the lower pressure differentials, i.e., at 10^{-2} mm Hg. This drift was demonstrated to originate in the transducer and not in the circuitry. When the transducer was replaced with a fixed resistor the drift was negligible. When PT#14 was used with a bridge circuit read-out, a similar drift and a similar data spread was observed.

The forward characteristics of another transducer, PT#9, that yielded good experimental results are illustrated in Fig. 26 for $\Delta P = 0$. The sensor (S#123) used in the fabrication of PT#9 had excellent characteristics as illustrated in Fig. 27. This transducer was also fabricated in the

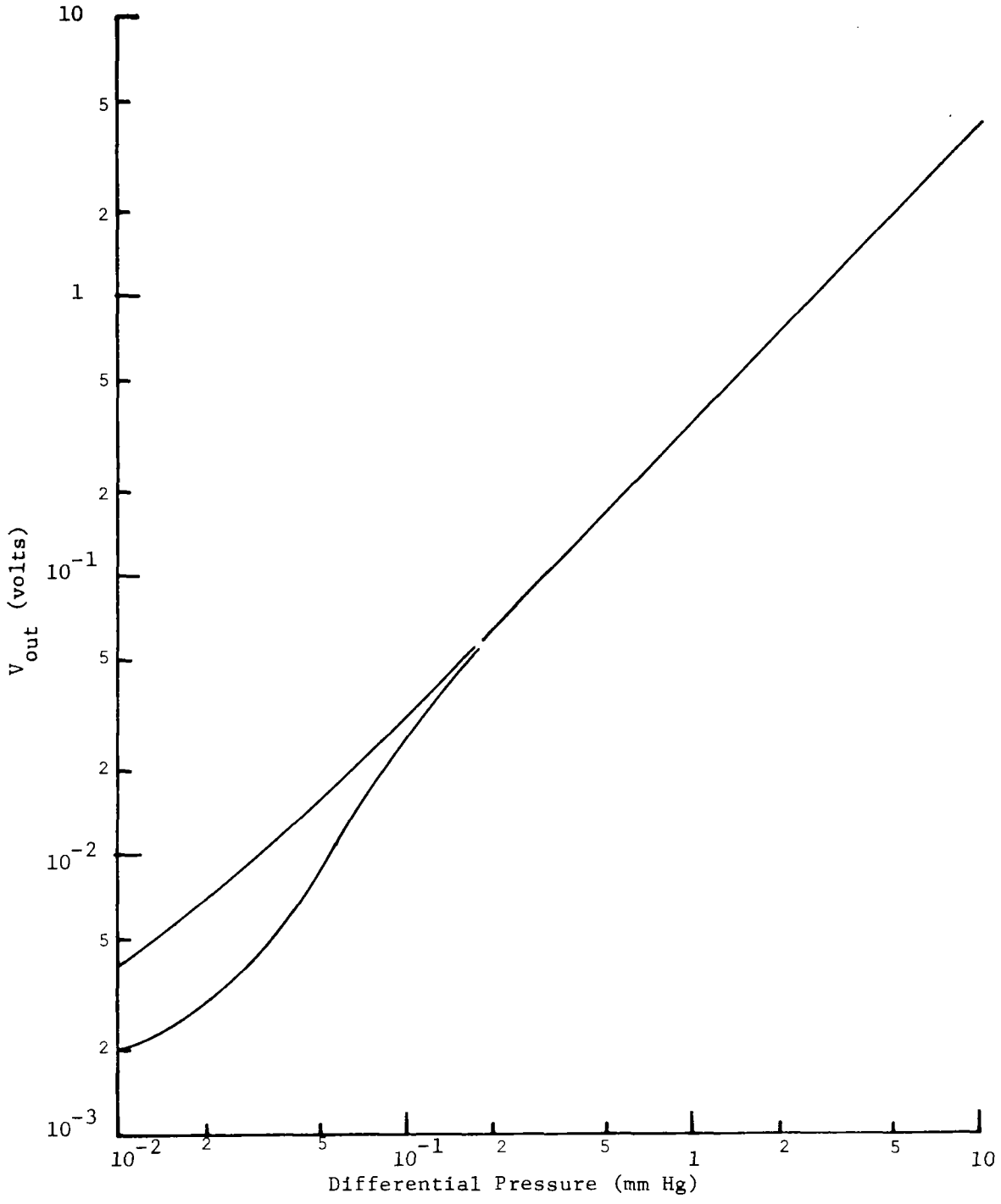

Figure 24. Read-out Voltage vs. Differential Pressure, PT#14

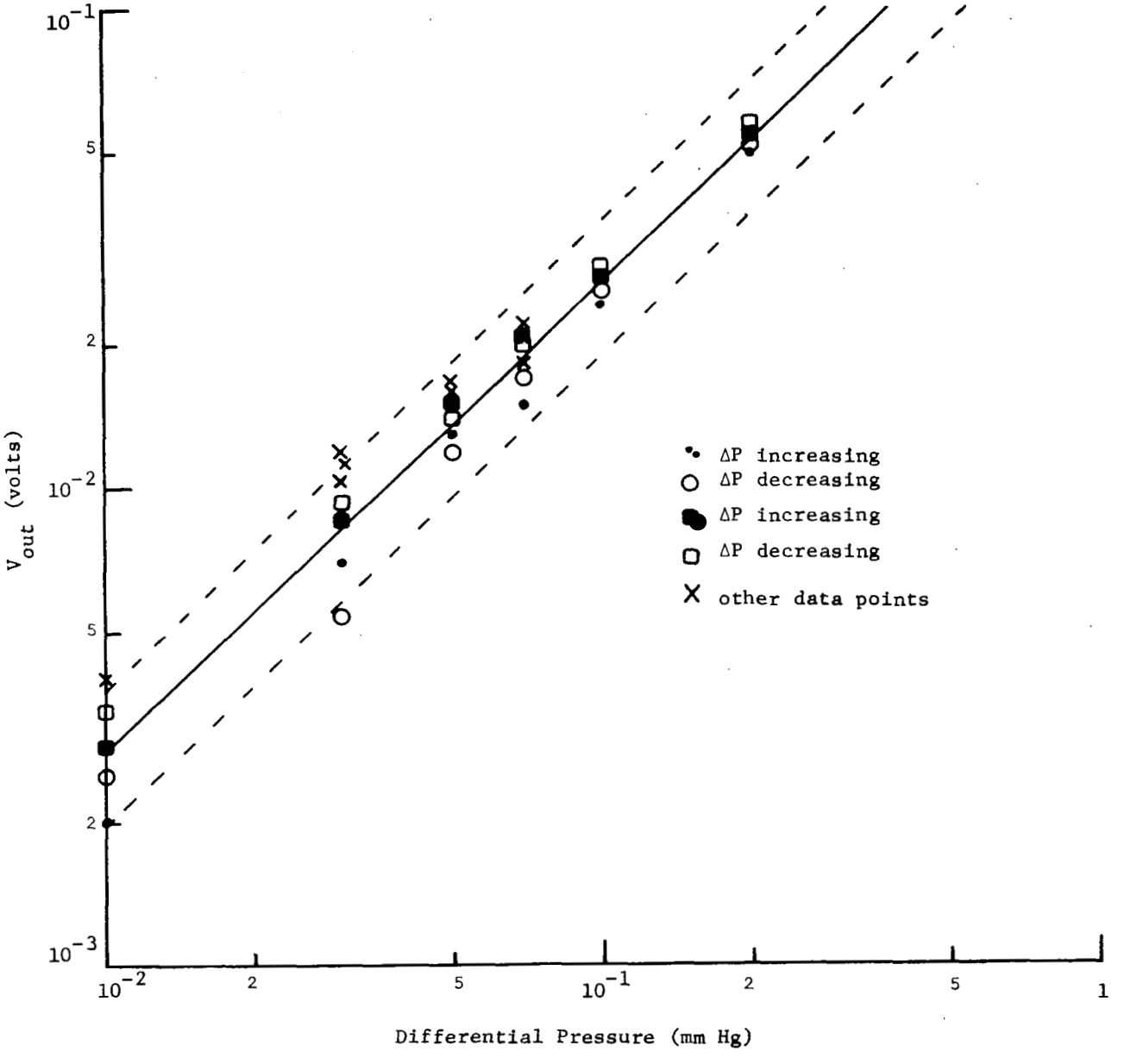

Figure 25. Low Pressure Characteristics of PT#14

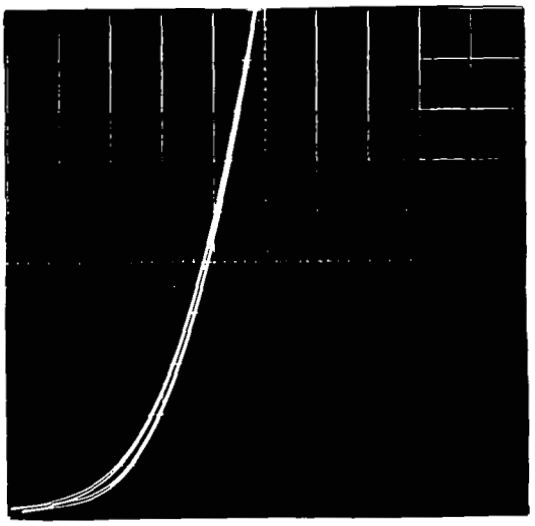

Figure 26. Forward V-I Characteristics of a Pressure Transducer (PT#9) with $\Delta P = 0$

Vertical: 0.05 V/div.
Horizontal: 0.01 mA/div.

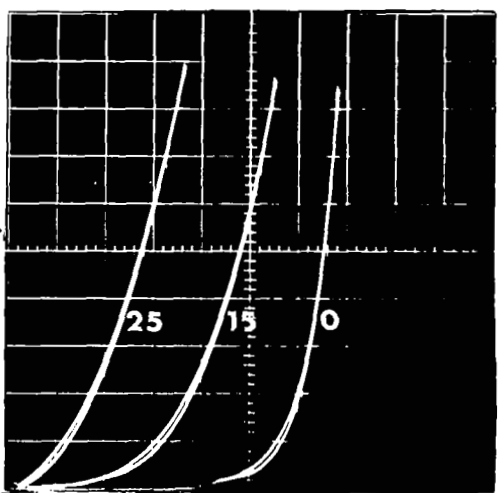

Forward

Vertical: 0.01 mA/div.
Horizontal: 0.05 V/div.
F = 0
≃ 15g
≃ 25g

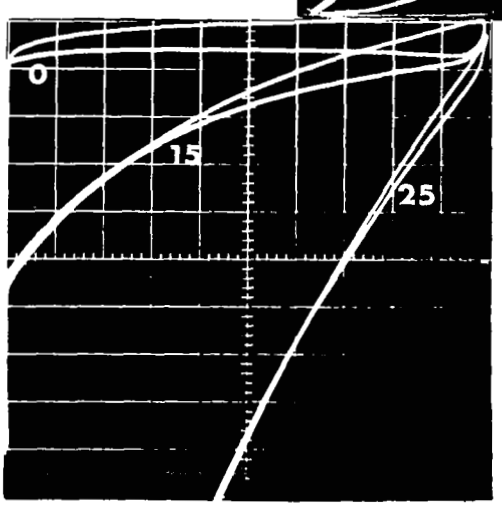

Reverse

Vertical: 0.01 mA/div.
Horizontal: 1.0 V/div.
F = 0
≃ 15g
≃ 25g

Figure 27. V-I-Stress Characteristics of a Needle Sensor (S#123)

standard housing with the 2.5 mil thick and 7 mm radius silicon diaphragm. The circuit shown in Fig. 23 was used to test this transducer. With a zero differential pressure the variable power supply was adjusted such that the forward voltage dropped across the transducer was 0.3 volts and the potentiometer was adjusted to zero the amplifier output. The transducer was evaluated by varying the pressure cross the transducer and recording the amplifier output. Data recorded from these experiments are illustrated in Fig. 28. Above 0.5 mm Hg the data was readily repeatable. Below this pressure, a significant variation occurred as illustrated in Fig. 28. The return path for a given pressure cycle was not consistently above the output voltage for the increasing pressure path, but this tended

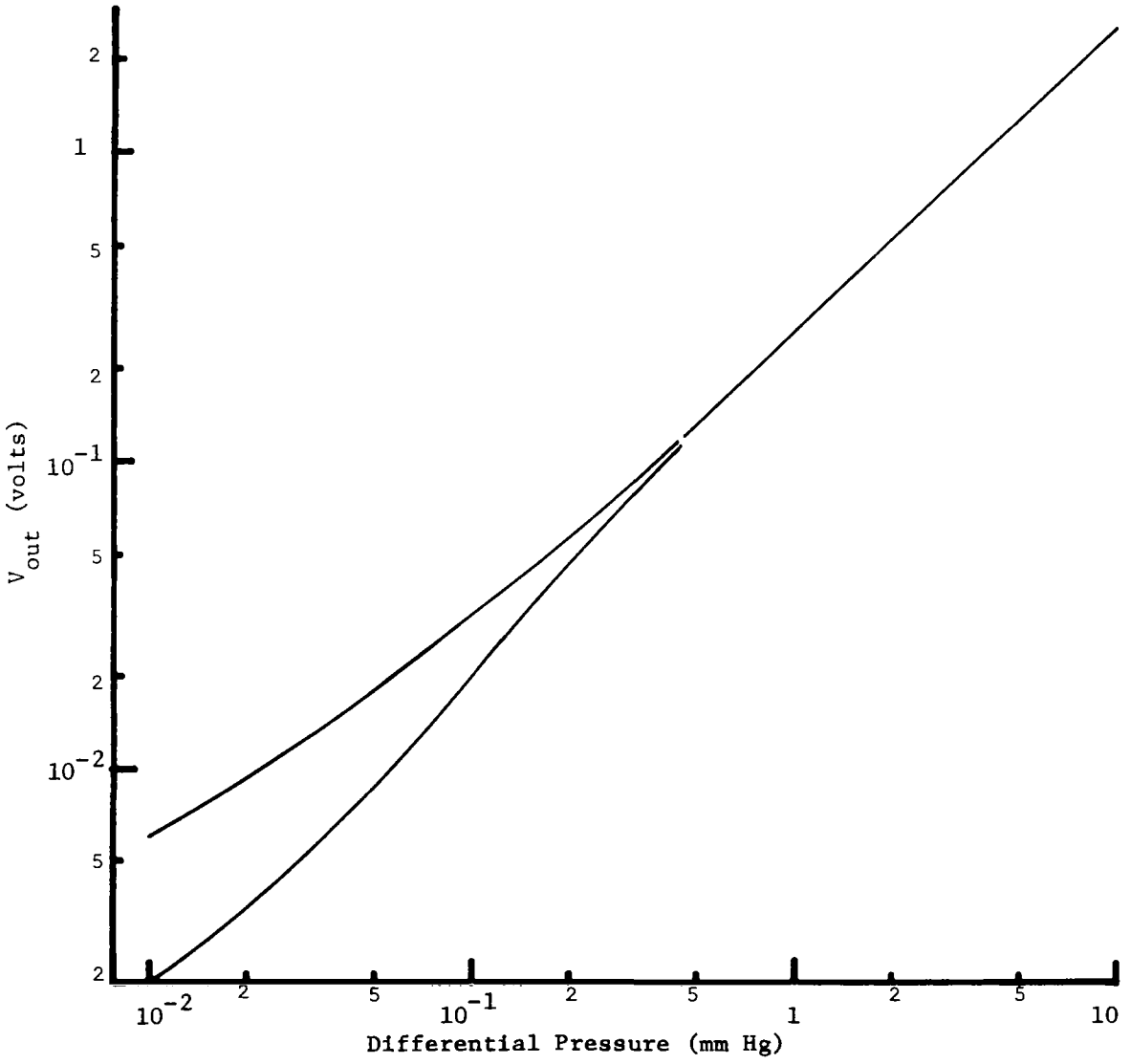

Figure 28. Read-out Voltage vs. Differential Pressure, PT#9

to be the case. This experiment was repeated at room temperature over a period of several weeks with similar results. When the transducer was placed in a low temperature environment, -50°C, and returned to room temperature, the transducer's characteristics had changed and it tended to be less stable.

A more typical transducer than either PT#9 or PT#14 is PT#8. The sensor (S#111) used in the fabrication of this transducer was relatively leaky. However, it was sensitive to stress and the forward V-I characteristic was stable. The V-I-stress characteristics of S#111 are illustrated in the oscillograms of Fig. 29. The fabrication techniques were standard and the silicon diaphragm was 2.5 mils thick and 7 mm in diameter. The read-out circuitry used with PT#8 is illustrated in Fig. 30. A bridge of this type was frequently used as a read-out circuit; it required a minimum

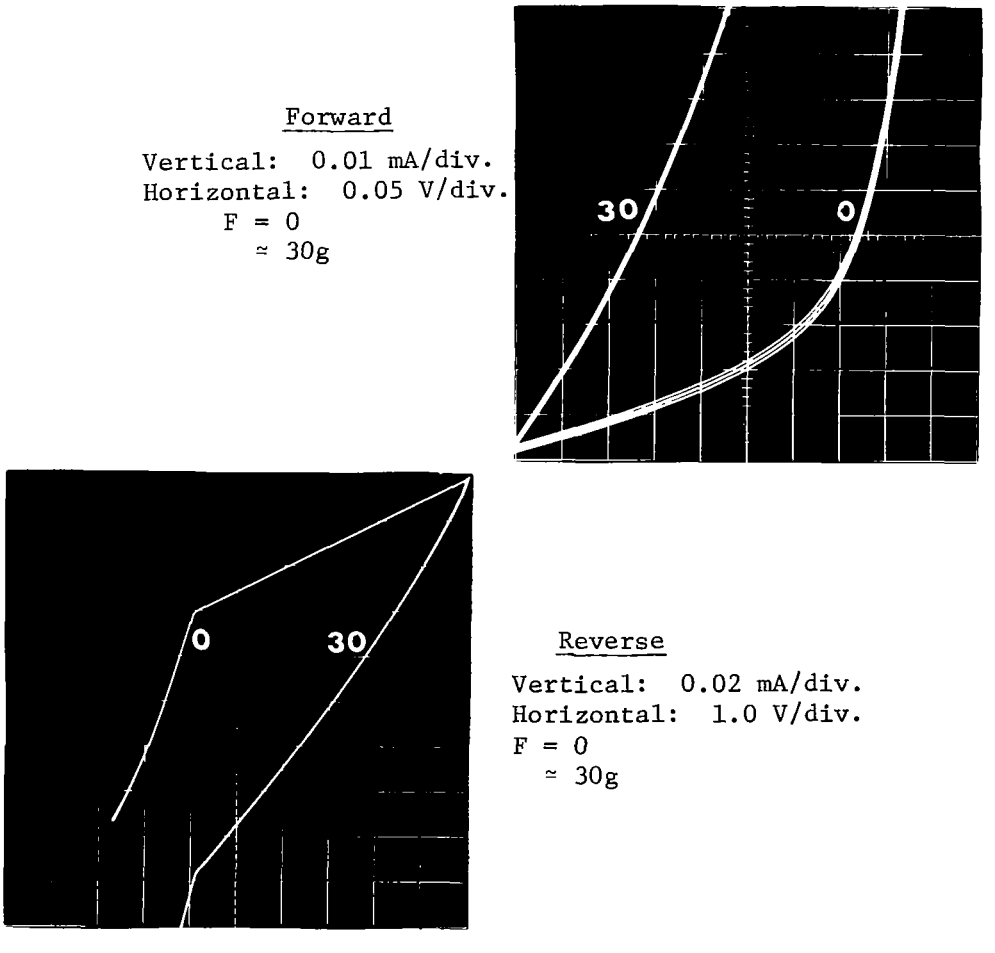

Figure 29. V-I-Stress Characteristics of S#111

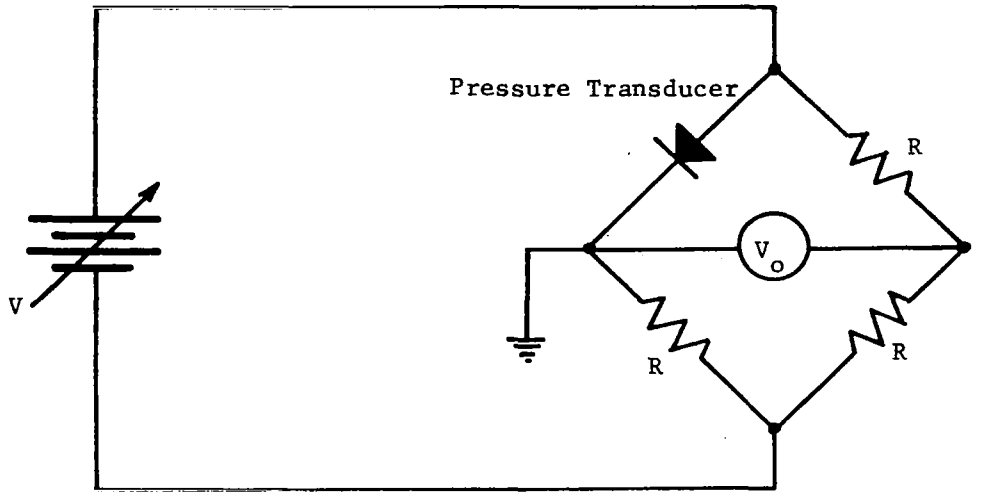

(R = Pressure Transducer Impedance at Operating Point)

Figure 30. Bridge Read-out Circuit for a Pressure Transducer

of additional components and provided adequate resolution. By replacing the transducer in the bridge with a fixed resistor, the bridge was observed to be very stable.

The characteristics of PT#8 are illustrated in Fig. 31. The significant feature of this transducer is that when the pressure was increased and then decreased, the output voltage was consistently higher on the return-to-zero portion of the cycle. If the pressure was cycled a second time, the output voltage tended to follow the initial return path; i.e., path B in Fig. 31, as pressure was increased and returned by way of a still higher voltage. This was characteristic of most of the transducers fabricated.

The output voltage plotted in Fig. 31 is an absolute value. The voltage measured was actually negative when an increase in pressure corresponded to an increase in stress on the silicon needle sensor, and was positive when an increase in pressure corresponded to a decrease in stress. These are the expected responses. In the experiment illustrated in Fig. 31, an increasing pressure corresponded to an increasing stress. When a differential pressure was applied such that an increasing pressure reduced the stress applied to the needle sensor, the response remained as illustrated; i.e., the output voltage increased from zero to a positive output and returned by way of a more positive voltage when the pressure was reduced.

Several pressure transducers were fabricated that were unique in some physical feature. One such unit had a large corregated metallic diaphragm with a small silicon chip bonded to its center. This unit was the most sensitive fabricated, but its repeatability was very poor. It could

readily be used as a microphone, but was unsuitable for constant pressure measurements. Diaphragms 5 to 7 mils thick of both silicon and quartz were used in transducers. These generally tended to be less sensitive than transducers with thin diaphragms without a significant improvement in other aspects.

A basic limitation characteristic of all the transducers is a limited dynamic range. This limitation is particularly serious in view of the need for an absolute pressure transducer. Transducers that will function at low differential pressures, e.g., 10^{-2} mm Hg, have to be mechanically biased into the stress-sensitive region and the stress added by an atmosphere of pressure will damage the sensor. An absolute transducer which could withstand an atmosphere of pressure was fabricated as follows: the housing was assembled complete with diaphragm but without the Cajon fitting on the sensor side of the housing. The completed portion of the housing was pressurized to two atmospheres absolute, and the silicon needle sensor was placed in position and stressed to the maximum. Finally, pressure was relieved from the complete side of the housing and the epoxy bonding the needle permitted to cure. Evacuating the sensor-side of the completed transducer resulted in an absolute unit. These transducers were not satisfactory, however. As pressure was reduced in the diaphragm-side of the transducer, the diaphragm insufficiently stressed and then lost physical contact with the needle sensor. In one such unit, for example, the transducer was no longer sensitive to pressure changes after the pressure was reduced to approximately 360 mm Hg in the diaphragm-side of the housing.

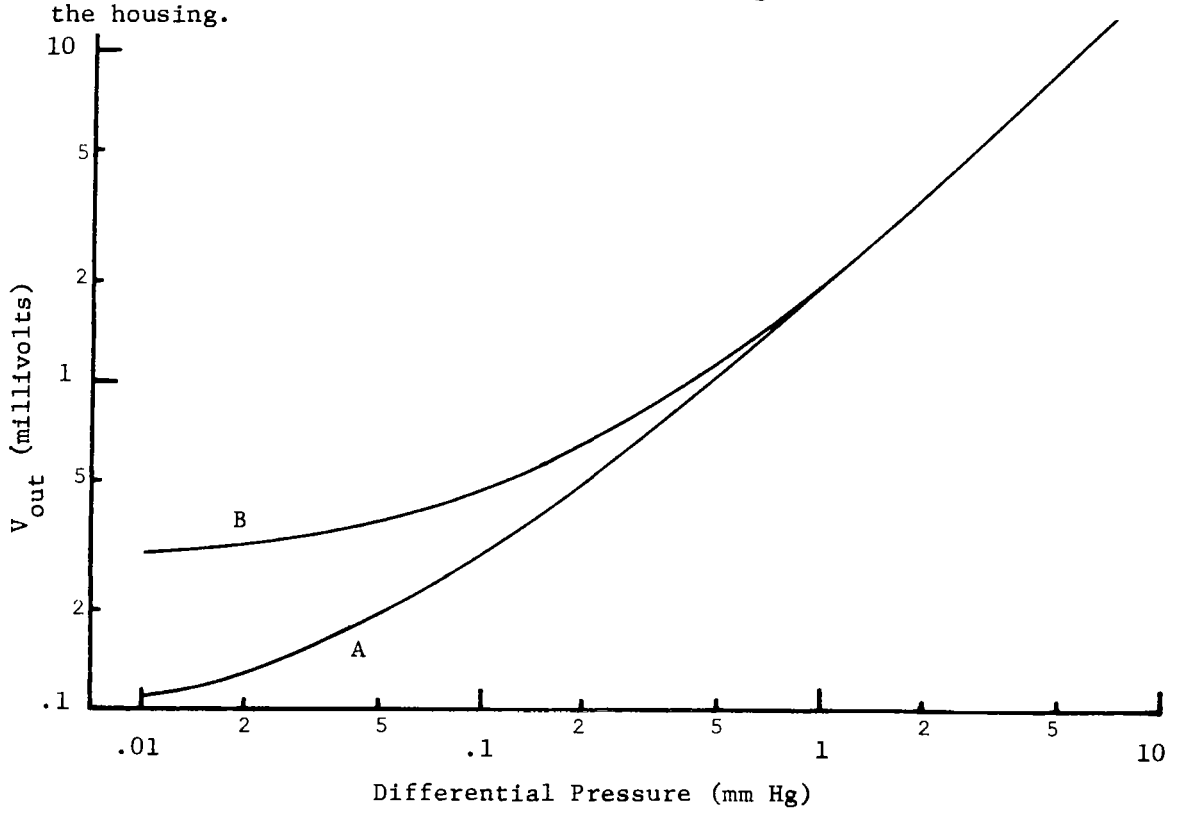

Figure 31. Read-out Voltage vs. Differential Pressure, PT#8

Discussion of results. - All of the data presented in the preceding section were recorded at room temperature which was reasonably constant over the periods of time required to observe drift or to make an experimental run. Furthermore, the observed drift was not always in the same direction. Consequently, temperature variations are concluded not to be the source of drift and lack of repeatability observed in the experimental data. Self-heating due to an internal power dissipation can also be dismissed as a probable cause. Several experiments were run in which the bridge circuit and transducer were electrically excited only when a data point was to be read and the results were similar to those achieved when electrical excitation was constantly applied. Also, the drift was not a problem at the high current levels corresponding to high stress.

The most probable source of the zero error in transducers such as PT#8 is creep in the housing. When a differential pressure is applied such that the stress on the sensor is increased, for example, the zero shift is in a direction that corresponds to an increased stress. When the applied pressure is caused to decrease the stress applied to the sensor, the zero shift corresponds to a decreased stress. The output voltage which exists after the differential pressure has been cycled does not drift back to zero. Generally, the drift that follows such an experiment tends to be small relatively to the zero error that has accumulated and it is as likely to increase as to return towards zero. It has been the experience of some manufacturers that a pre-stressed diaphragm was essential to zero stability and low hysteresis. This suggests that a prestressed diaphragm may provide for significant improvements in transducers such as PT#8.

Several transducers changed characteristics during testing. In some instances, these units were inadvertently exposed to excess pressure differentials. In other cases, the reason for the change is not obvious. The needle sensor from some of these transducers were recovered from the transducer housing and examined for damage. Usually, the sensor tip was found to be chipped.

The problem of damage and damage propagation at the sensor tip could benefit from additional experimental efforts. The usual practice with completed sensors was to view their V-I characteristics on a curve tracer and then apply an increasing stress to evaluate the sensitivity of the sensors. This same procedure was applied to the sensors that had good reverse characteristics. It is probable that a reverse leakage of 1 μA could not be observed on the curve tracer and, consequently, it is possible that the reverse leakage of a good sensor changed several orders of magnitude with increasing stress before it was observed on the curve tracer.

It is unfortunate that the better sensors were not instrumented adequately to observe the reverse leakage at zero stress.

Other needed investigations were not completed due to a shortage of needle sensors. Experimental evaluations of diaphragm size and material were inconclusive and investigations of bonding materials and environmental effects were insufficient. An increased supply of suitable needle sensors will make these investigations possible.

The Simple Diaphragm

In the simple diaphragm configuration, a pressure differential across a silicon diaphragm stresses a p-n junction fabricated in the center of the diaphragm. This configuration, illustrated in Fig. 32, has the advantages of mechanical simplicity, achieving large-area stresses, and ease of fabrication with silicon planar technology. Problem areas such as creep, alignment, and hysteresis which are associated with the mechanical housing are reduced in this simple configuration and, as illustrated in Sect. II, it is advantageous to stress the entire junction area. Regardless of these advantages, the simple diaphragm configuration is concluded to be inadequate as a sensitive pressure transducer. Extremely large pressure biases are required to achieve stresses in the diaphragm on the order of 10^9 dynes/cm^2. Thin diaphragms in which large deflections can occur have an additional disadvantage in that the diaphragm stresses are tensional rather than compressional. A comparison of Figs. 3 and 4 of Sect. II illustrate that the compressional stress is more desirable since $\gamma_v(e)$ is significantly greater for a given compressional stress than tensional stress. In a practical-sized, thin silicon diaphragm, e.g., a radius of 0.28 inches and a thickness of 2.5×10^{-3} inches, it has been demonstrated

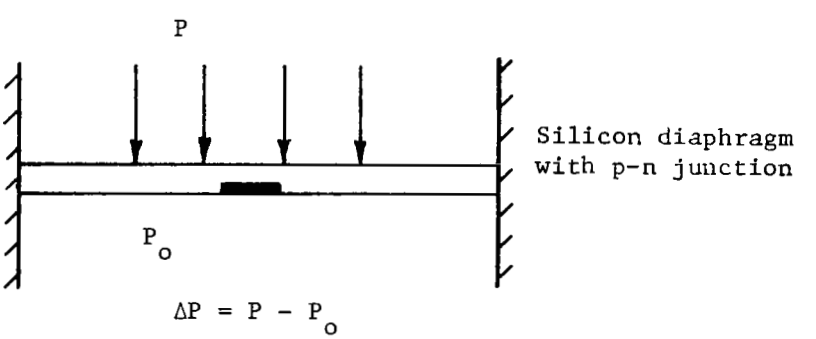

Figure 32. The Simple Diaphragm Pressure Transducer

that a pressure differential of more than 2×10^3 mm Hg is required to achieve a diaphragm stress of 5×10^9 dynes/cm^2 (Ref. 1). In relatively thick diaphragms in which large compressional stresses can be achieved, even greater differential pressures are required. If diaphragm thickness is assumed to be about 1/4 of the radius, a pressure differential of approximately 1.5×10^3 mm Hg is required for a compressional stress of 10^9 dynes/cm^2. Larger pressure differentials result in a "ballooned" diaphragm and tensional stresses. If the ratio of thickness to radius is reduced, the diaphragm will "balloon" to a tensional stress at a lower differential pressure. These conclusions are based upon the results of Roark (Ref. 8).

The Indenter-Point Configuration

The indenter-point configuration is the inverse of the needle sensor configuration, i.e., the p-n junction is fabricated in a planar surface and a needle or pin is used to stress the junction area. Two indenter point configurations are illustrated in Figs. 33 and 34. In Fig. 33, the differential pressure is applied across a silicon diaphragm and the p-n junction in the diaphragm is stressed against the indenter-point. In Fig. 34, the p-n junction is fabricated in a silicon chip which is rigidly bonded to the transducer housing, and the indenter is forced against the chip by a separate diaphragm. The piezojunction phenomenon has been observed in both configurations. It has not been observed in a configuration similar to Fig. 33 when the p-n junction was on the opposite side of the diaphragm from the indenter-point.

The force applied by the indenter-point to the p-n junction area is approximately

$$F = F_o + \frac{\Delta P \pi a^2}{4} \tag{19}$$

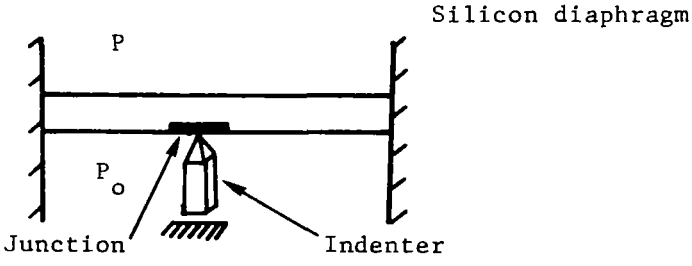

Figure 33. The Indenter-Point Pressure Transducer Configuration

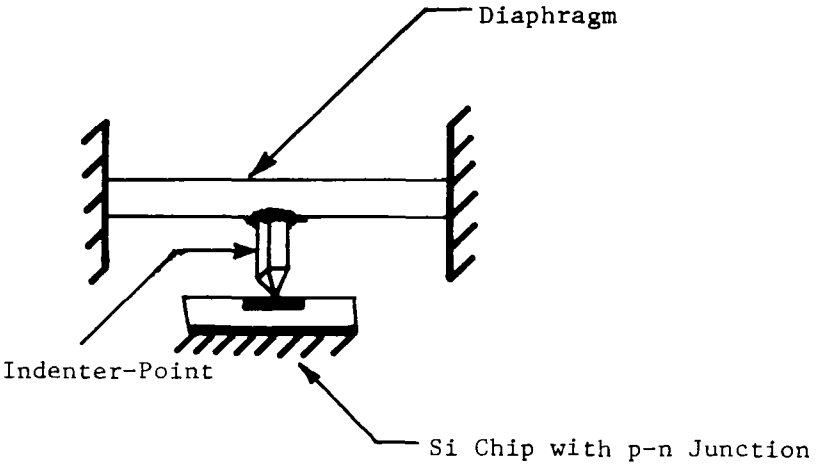

Figure 34, The Indenter-Point Transducer with Junction in Chip

where F_o = bias force when $\Delta P = 0$,

ΔP = pressure differential across diaphragm, and

a = diaphragm radius.

The stress applied to the diaphragm by the indenter-point is a function of the force and the area of the indenter-diaphragm contact (Ref. 1).

The indenter-point configuration has all the disadvantages of the silicon needle sensor configuration including a relatively complex housing and a mechanical contact to the junction area. Additionally, it has an alignment problem during fabrication which is difficult to overcome. In the event of misalignment it is likely that only a small portion of the junction area will be stressed and the piezojunction sensitivity significantly reduced. The single advantage of the indenter-point configuration over the needle sensor is that the p-n junction fabrication is a direct application of planar processing technology.

Other Transducer Configurations

Transducer configurations which have not been experimentally investigated include configurations utilizing multijunction devices such as transistors and four-layer switches. Generally, it is thought that the nonlinear V-I characteristics of a single p-n junction can be used to control a more complex structure and, consequently, should receive prior consideration. In the needle sensor configuration, the single junction structure must be perfected before more complex structures are attempted.

A pressure transducer which utilizes an indenter-point to apply stress to a transistor structure has been marketed commercially. This unit was investigated experimentally to evaluate its potential as a sensitive pressure transducer and a typical result is illustrated in Fig. 35. Additionally, the output drift over a period of 1 hour

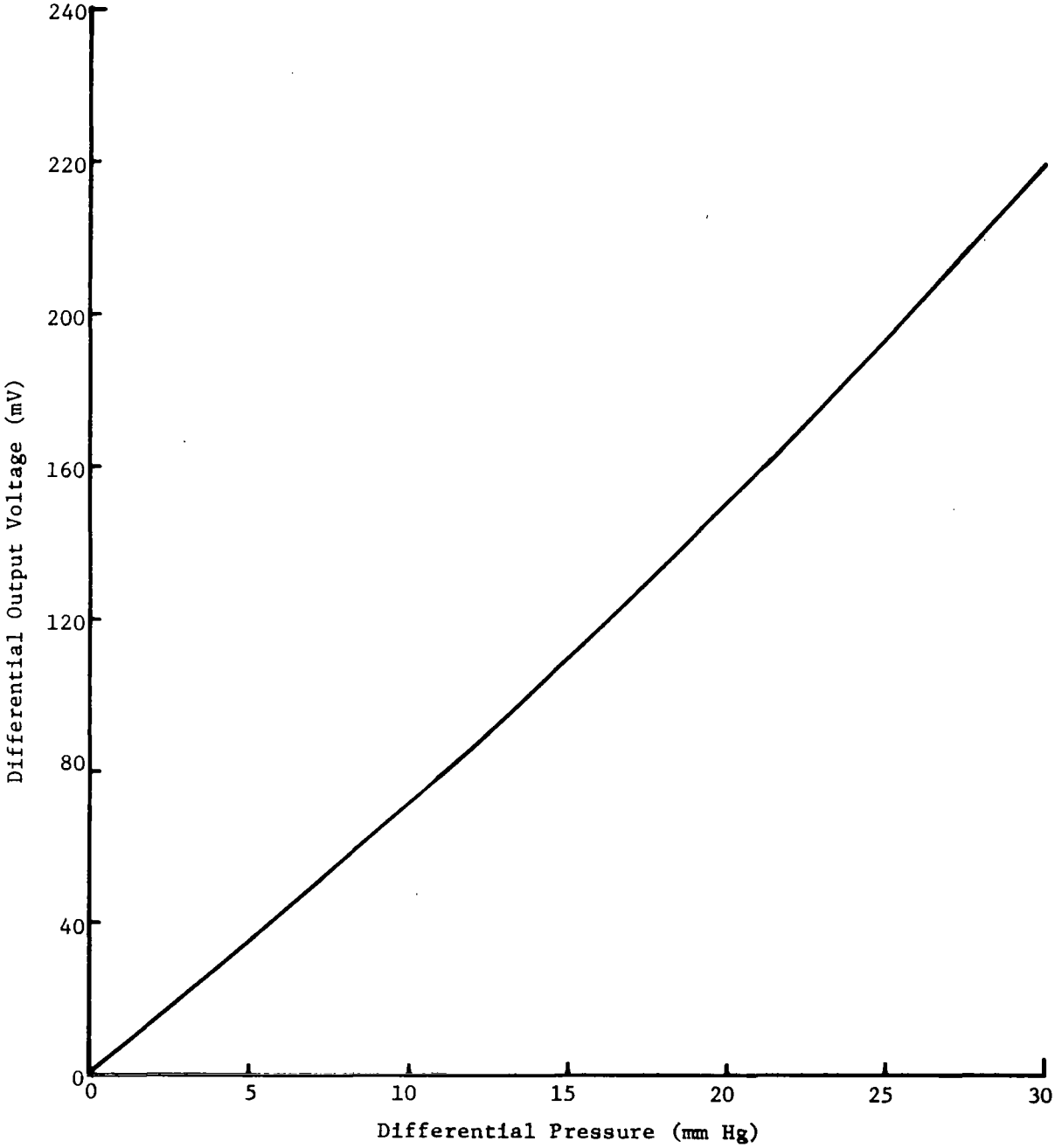

Figure 35. Output Voltage Pressure Characteristics of a Commercial Transducer Utilizing the Piezojunction Effect

correspond to approximately 7 mm Hg. The published specifications refer to differential pressures greater than those of interest here and the transducer could not reliably detect the low pressure differentials required, e.g., 10^{-1} mm Hg.

Read-out Circuitry

Read-out circuits used in the experimental portion of this investigation include amplifier circuits such as illustrated in Fig. 23, the bridge read-out circuit illustrated in Fig. 30, the bridge circuit of Fig. 30 with an operational amplifier connected across V_{out}, classical unijunction oscillator circuits such as illustrated in Fig. 36, and a bridge circuit utilizing two diodes and ac excitation such as illustrated in Fig. 37. For laboratory conditions, the simple bridge of Fig. 30 with a dc differential voltmeter was the most useful, and it provided adequate read-out resolution for any of the transducers tested. For a constant supply voltage, the transducer forward-bias voltage is reduced by the increase in current through the resistor in series with the transducer, but this is generally true of every dc circuit considered.

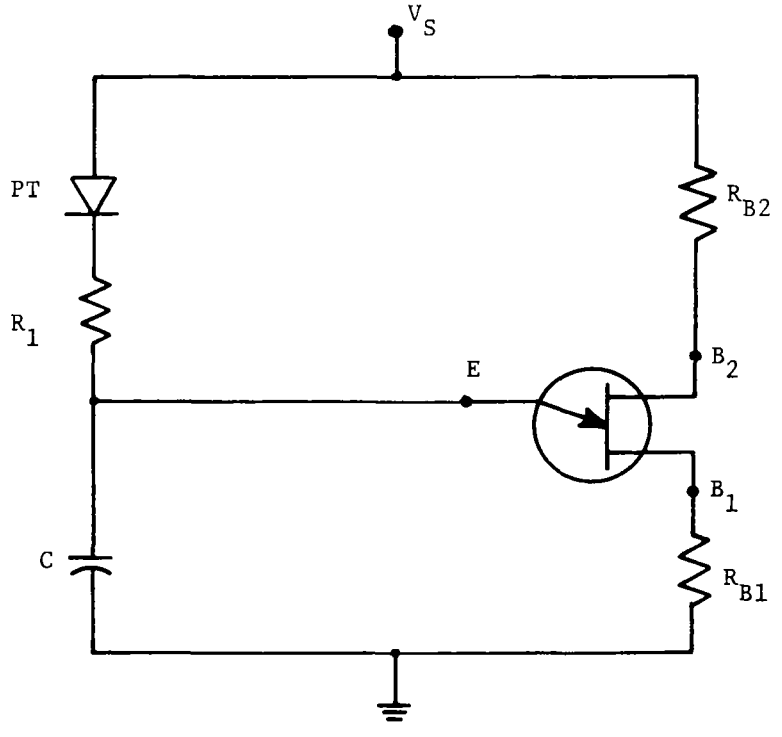

Figure 36. A Unijunction Oscillator Read-out Circuit

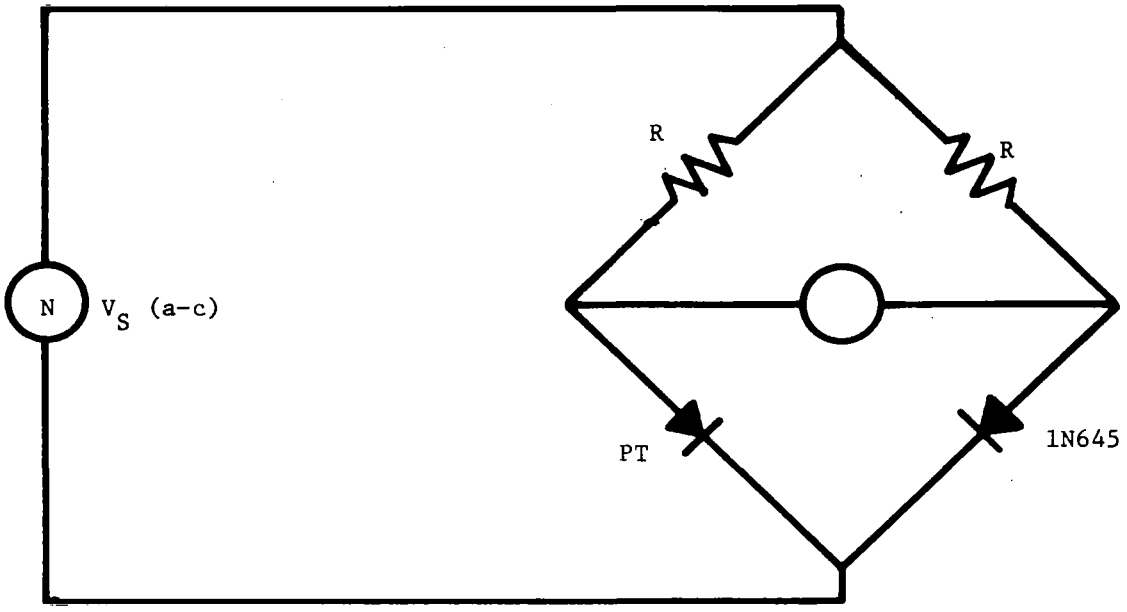

Figure 37. A Diode-Resistor Bridge Read-out Circuit

For low differential pressure outputs, the amplifier circuits required stable amplifiers with low offset drift. Such amplifiers are readily available; however, most amplifiers will require periodic adjustment of the dc offset.

The unijunction oscillator circuits such as illustrated in Fig. 36 were generally unsatisfactory. The emitter-base one voltage drop for the unijunction is usually greater than the desired forward bias of the transducer, and the forward impedance of the transducer must be appreciable with respect to R_1 in order for its change with pressure to be significant. Consequently, the supply voltage had to be relatively low and it was difficult to meet the conditions required for oscillation (Ref. 9). Several transducers were operated with unijunction read-out circuits and these tended to be insensitive.

The ac bridge circuit of Fig. 37 was used in an attempt to eliminate dc drift in the transducer read-out. Results were compromised by the lack of matched forward and reverse characteristics in the diodes. An ideal arrangement would utilize two matched transducers as the diodes in Fig. 37, one reduced in stress by the applied pressure and the other increased in stress by the applied pressure. The oscillograms of Fig. 38 illustrate the output of a bridge circuit such as Fig. 37. The diodes were PT#9 and a 1N645.

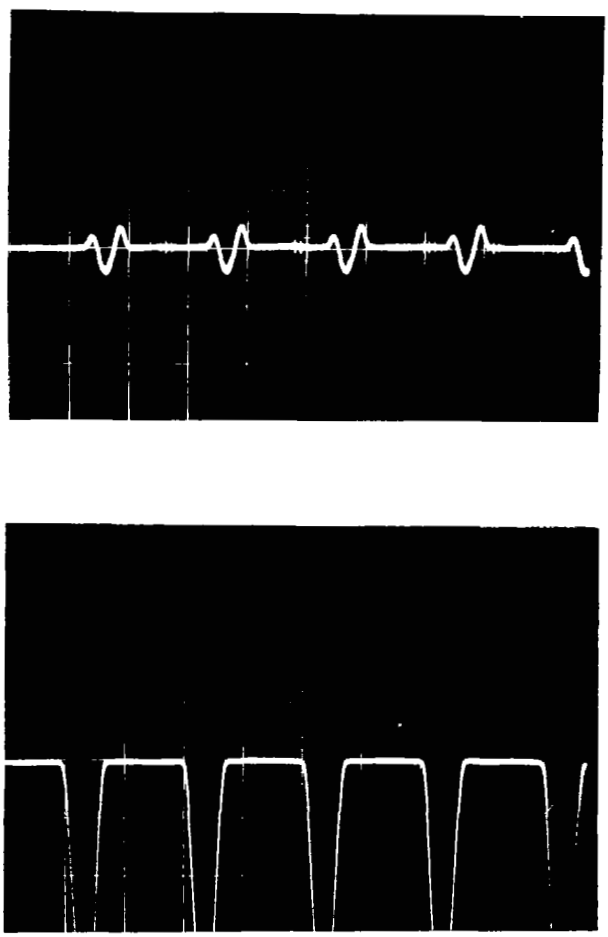

Figure 38. Output Voltage of the Diode-Resistor Bridge Circuit for ΔP = 0 and ΔP = 10 mm Hg

SECTION IV

CONCLUSIONS AND RECOMMENDATIONS

During the course of this investigation, significant progress was made toward the development of piezojunction transducers. Sensitive silicon needle sensors were fabricated with excellent p-n junction characteristics, and these were used in pressure transducers with encouraging results. These results demonstrate the feasibility of utilizing the sensitive, piezojunction phenomenon in a small, solid-state pressure transducer. This is an excellent beginning; however, much development remains to be done.

Because of the many advantages of the needle sensor configuration, much of the effort of this study was directed toward the development of a process for fabricating these sensors. Although the yield of sensors remained low and actually compromised the total results of this investigation, it is very probable that a high-yield facility will evolve. In view of developments that have occurred in other areas of semiconductor processing, there is every reason to expect the eventual development of an automated, high-yield facility producing consistently good-quality needle sensors. It is also reasonable to expect the sensor quality to improve so as to yield more sensitive devices.

The transducers fabricated during this investigation were limited in number by the low yield of needle sensors. Transducers were fabricated, however, which resolved differential pressures of 10^{-2} mm Hg. The usefulness of these transducers were limited by zero error, drift and a lack of repeatability at the lower pressures. These limitations are likely to be characteristic of the housing configuration rather than the needle sensor or the piezojunction phenomenon. An adequate supply of needle sensors will provide opportunity for the development of an improved housing and an experimental program to evaluate the characteristics of the sensors independently of a housing.

The best transducers fabricated were not atypical, but they were similar to each other in that they utilized good quality needle sensors and the zero pressure stress-bias was relatively small. Typically, they used a thin silicon diaphragm which was not stressed when bonded to the transducer housing. It is reasonable to expect that significant improvements could be achieved through improved diaphragm design, and it is reasonable that good quality sensors and small initial stresses yielded the best experimental results. A transducer design for the needle sensor is in its infancy and will mature with an adequate supply of sensors.

While there is every reason to expect significant improvement in these transducers, there are factors that may limit their ultimate usefulness. The sensitive transducers fabricated during this investigation

were limited in the maximum differential pressure they could withstand. The high stress required for the piezojunction phenomenon to occur is close to the fracture stress of silicon, and the sensors are easily damaged by small increases in stress. This factor does not limit sensitivity, however, and the sensitivity can be traded-off for dynamic range. These transducers are also sensitive to temperature since this is inherent in the p-n junction, and temperature compensation will be required in most applications. The output of the piezojunction transducers also tends to be small, i.e., on the order of the forward voltage across the p-n junction; however, this is characteristic of most sensitive transducers.

The experimental results achieved in this investigation represent a good beginning. Sensitive pressure transducers utilizing the piezojunction phenomenon were fabricated. These results are not conclusive, however. The low yield of needle sensors limited the experimental evaluation of various attributes of the complete transducer assembly and additional efforts in this phase of the development are needed. It is concluded that an adequate supply of needle sensors would quickly yield significant improvements in the piezojunction pressure transducers, and that an effort to obtain such a supply is warranted.

APPENDIX A

THE RELATIONSHIP OF STRESS TO STRAIN

Strain and stress are related through Hook's generalized law,

$$[e_{ij}] = [S_{ij}]\,[\sigma_{ij}]\ , \tag{A-1}$$

where

e_{ij} = strain components,

σ_{ij} = stress components, and

S_{ij} = stiffness coefficients for the crystal.

For the case of the cubic, silicon crystal, Hook's generalized law is (Ref. 5)

$$\begin{bmatrix} e_1 \\ e_2 \\ e_3 \\ e_4 \\ e_5 \\ e_6 \end{bmatrix} = \begin{bmatrix} S_{11} & S_{12} & S_{12} & 0 & 0 & 0 \\ S_{12} & S_{11} & S_{12} & 0 & 0 & 0 \\ S_{12} & S_{12} & S_{11} & 0 & 0 & 0 \\ 0 & 0 & 0 & S_{44} & 0 & 0 \\ 0 & 0 & 0 & 0 & S_{44} & 0 \\ 0 & 0 & 0 & 0 & 0 & S_{44} \end{bmatrix} \begin{bmatrix} \sigma_1 \\ \sigma_2 \\ \sigma_3 \\ \sigma_4 \\ \sigma_5 \\ \sigma_6 \end{bmatrix} . \tag{A-2}$$

With respect to notation, e_1, e_2 and e_3 are the principal strains e_{xx}, e_{yy} and e_{zz}; e_4, e_5 and e_6 are the shear strains e_{yz}, e_{xz} and e_{xy}; and

$$e = e_1 + e_2 + e_3\ . \tag{A-3}$$

With a general stress applied to a crystal, it is possible to evaluate the principal (with respect to the crystal axes) and shear strains. The strain components resulting from a stress are necessary for calculating $\gamma_\nu(e)$. For a hydrostatic stress of magnitude T,

$$\sigma_1 = \sigma_2 = \sigma_3 = -\,T\ , \text{ and} \tag{A-4}$$

$$\sigma_4 = \sigma_5 = \sigma_6 = 0\ .$$

From Hook's Law, the strain components are computed as

$$e_1 = e_2 = e_3 = - (S_{11} + 2\ S_{12})T, \text{ and}$$
$$e_4 = e_5 = e_6 = 0 \ . \tag{A-5}$$

For a uniaxial [111] stress of magnitude T,

$$\sigma_1 = \sigma_2 = \sigma_3 = \sigma_4 = \sigma_5 = \sigma_6 = - T/3 \ , \tag{A-6}$$

$$e_1 = e_2 = e_3 = - T(S_{11} + 2\ S_{12})/3 \ , \text{ and}$$
$$e_4 = e_5 = e_6 = - T\ S_{44}/3 \ . \tag{A-7}$$

For a uniaxial [011] stress of magnitude T,

$$\sigma_1 = 0 \ ,$$
$$\sigma_2 = \sigma_3 = - T/2 \ ,$$
$$\sigma_4 = - T/2, \tag{A-8}$$
$$\sigma_5 = \sigma_6 = 0 \ ,$$

$$e_1 = - S_{12}\ T \ ,$$
$$e_2 = e_3 = - T(S_{11} + S_{12})/2 \ ,$$
$$e_4 = - T\ S_{44}/2 \ , \text{ and} \tag{A-9}$$
$$e_5 = e_6 = 0 \ .$$

For a uniaxial [100] stress of magnitude T,

$$\sigma_1 = - T \ ,$$
$$\sigma_2 = \sigma_3 = \sigma_4 = \sigma_5 = \sigma_6 = 0 \ , \tag{A-10}$$

$$e_1 = - S_{11} T ,$$

$$e_2 = e_3 = - S_{12} T , \text{ and} \qquad \text{(A-11)}$$

$$e_4 = e_5 = e_6 = 0 .$$

In the preceding equations the applied stress, T, is positive when compressional, and negative when tensional (Ref. 5).

The stiffness coefficients of silicon, S_{ij}, of Eq. (A-2) are given by Mason (Ref.10) as follows:

$$S_{11} = 0.768 \text{ cm}^2/10^{12} \text{ dynes},$$

$$S_{12} = - 0.214 \text{ cm}^2/10^{12} \text{ dynes, and}$$

$$S_{44} = 1.26 \text{ cm}^2/10^{12} \text{ dynes.}$$

APPENDIX B

NEEDLE FABRICATION PROCEDURE

The needle fabrication procedure described in this Appendix evolved from much experimental work in all phases of the fabrication process. The starting point was a needle sensor shaped by electrochemically etching and diffused through a single window opened in the passivating oxide. The resulting needle sensor was unsatisfactory for numerous reasons: the nonuniform tips tended to be too fragile to survive the necessary handling during fabrication and testing, the p-n junction characteristics were masked by the characteristics of the mechanical contact required to establish electrical contact to the tip region of the needle sensor, the diffusion window opening tended to be ragged and poorly defined, and the passivating oxide tended to be of poor quality due to the condition of the bulk silicon surface. It was essential that the needle fabrication process be perfected to provide for a uniform geometry, a smooth surface, and a double window with a metallized contact to the tip region. These objectives were achieved and the process yeilding the silicon needle sensors is described in the following paragraphs. The starting point in the process description is a silicon bar approximately 50 mils square and 750 mils long. The principal axis is in the [100] direction and the resistivity is approximately 1 ohm-cm. These specifications are not critical. The physical dimensions are small, but still provide physical strength for the mechanical shaping that will follow and the applied stress tends to be isotropic rather than anisotropic lessening the significance of the directional properties of the phenomenon.

The steps in the needle sensor fabrication are tabulated in Table B-1. Each step is identified by number and described in detail in the following paragraph. Many of these steps are not critical and some variations will not significantly effect the end result. However, these procedures yielded consistently good silicon needle sensors in our laboratories. Those familiar with semiconductor processing will recognize the extension of silicon planar technology. It is probable that knowledgeable personnel with access to improved facilities can take many liberties with the procedures described herein and achieve significant improvements in the final product.

(1) Clean Bar: This initial cleaning process enhances the results of the etching procedure which follows. The needles are boiled in acetone approximately 15 minutes to remove any residue of wax left from the cutting operations that preceed processing. The remainder of the cleaning procedure is standard and is repeated many time during processing. This standard cleaning procedure is described below:

(a) Place needles in the cleaning fixture and immerse fixture and needles in H_2SO_4 at 100°C for approximately 15 minutes.

(The cleaning fixture is a quartz fixture designed to minimize handling of the needles during the cleaning. Because of its usefulness, a photograph of the fixture is shown in Fig. B-1.)

TABLE B-1

Process Steps for Fabricating a Needle Sensor

1. Clean bar
2. Etch bar
3. Grind point
4. Clean
5. Etch point
6. Buff point
7. Clean
8. Etch point
9. Clean
10. First oxidization
11. Mask
12. Clean
13. Diffusion
14. Etch
15. Second oxidization
16. Second mask
17. Etch
18. Clean
19. Evaporate aluminum
20. Alloy
21. Mask with wax
22. Etch
23. Nickel plate
24. Clean
25. Bond lead

(b) Rinse fixture and needles in flowing DI H_2O for one minute. Immerse fixture and needles in gently boiling DI H_2O for 5 minutes, and rinse in flowing DI H_2O for 5 minutes.

(c) Immerse fixture and needles in HNO_3 at 80°C for 15 minutes.

(d) Repeat Step (b).

(e) Immerse needles in gently boiling DI H_2O for 5 minutes, and rinse in flowing DI H_2O for 20 minutes.

(f) Immerse the needles in warm Transene for 5 minutes.

(g) Using clean tweezers, remove the needles from the needle cleaning fixture and blow each needle dry with N_2. Keep needles in Transene until they are removed for blowing dry. Load the dry needles immediately into a clean petri dish with clean filter paper and transfer as quickly as possible into the appropriate furnace boat. (Note: The maximum hold time is only the time necessary to blow the needles dry, place them on a furnace boat and place the boat in the profile flat zone of the furnace tube. Only visual inspection is permitted during the dry nitrogen blow off period. Any extra holding or handling at this stage requires a repeat of the entire cleaning process).

(2) Etch Bar: The needle bars are immersed for 20 seconds in an agitated etch solution consisting of 3 parts HNO_3 and 1 part HF.

(3) Grind Point: The initial point shaping is done by bringing the spinning needle into contact with a stationary copper plate at an angle of 60°. The needle is turning at approximately 10,000 rpm. The copper plate is coated with a 15 micron alumina grit. Grinding is terminated when the needle profile approximates the shape illustrated in Fig. B-2. This requires a judgment decision by an experienced, skilled operator.

(4) Clean: Boil the needles in acetone for 15 minutes and in TCE for 15 minutes. The remainder of this cleaning procedure is the standard procedure described in No. 1.

(5) Etch Point: The needles are etched in the solution of 3 parts HNO_3 and 1 part HF for 10 to 20 seconds as required to round the point and smooth the surface. The etch solution is caused to flow smoothly around a beaker and the needle is immersed into the etchant with the point headed directly into the etchant flow. The needles are held in the etchant by tweezers at the very back of the shank.

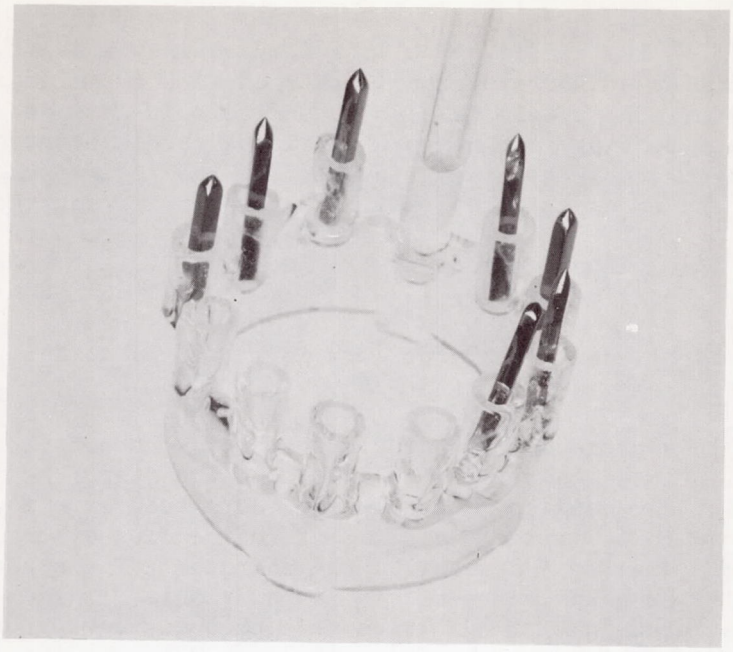

Figure B-1. A Photograph of the Needle Cleaning Fixture

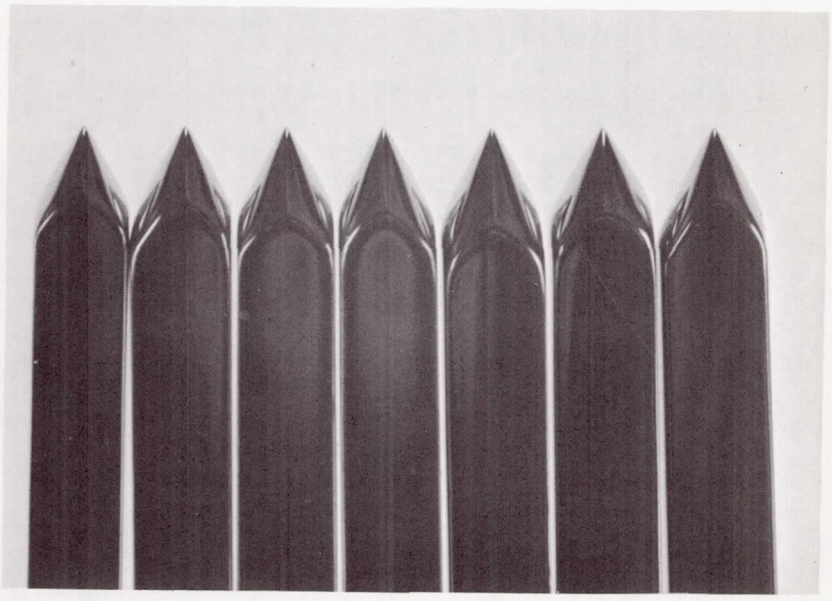

Figure B-2. A Photomicrograph of a Group of Silicon Needles Illustrating the Uniformity that can be Achieved in Mechanical Shaping

(6) Buff Point: The needle point is buffed against a 1 1/2" felt wheel turning at 1800 rpm and is charged with a 6 micron diamond grit paste. The needle is also caused to spin at approximately 1800 rpm. Buffing is continued until the needle point has acquired the desired shape. In Step (5) and (6), a judgement decision by an experienced, skilled operator is required.

(7) Clean: This cleaning procedure is identical to the cleaning procedure described in No. (4).

(8) A Final Etch: This etch procedure is identical to the procedure described in No. (5).

(9) Clean: This procedure is identical to the standard procedure of No. (1). At the conclusion of this cleaning step, the mechanical shaping of the needles is completed. As noted, several of these steps require individual handling of the needles by an operator, and also a quality judgement by the operator. The extent to which uniformity of shape was achieved is remarkable. This uniformity is illustrated in Fig. B-2 which is a photomicrograph of a group of 7 needles which were mechanically shaped from a lot of 8.

(10) First Oxidization: Place the cleaned needles in an oxidation furnace at 1100°C and grow a 10,000 Å oxide. A dry-wet-dry oxidation procedure is used as follows: 10 minutes in O_2 at 1000 cc per minute; 115 minutes in steam and 20 minutes in O_2 at 1000 cc per minute.

(11) Mask: The masking procedure is as follows:

(a) Preheat the needles in an oven and dip the still warm needles into a container of KPR to a point about half way up the shank three times.

(b) Heat the needles in an oven at 85°C for 15 minutes.

(c) Melt apiezon black wax on a glass slide and pull a second slide over the wax so as to obtain a very thin layer.

(d) Using a special spring holder, hold the tips of the needles against the wax-coated slide for one minute.

(e) Lift the needles free of the wax and allow to air dry for 2 minutes.

(f) As before, dip the needles into the container of KPR three times and air dry for ten minutes.

(g) Repeat Steps (d) and (e).

(h) Expose each needle under UV light for four minutes.

(i) Develop in TCE for 2.5 minutes.

(j) Bake at 160°C for 15 minutes.

(k) Etch in buffered HF for 7 minutes.

(l) Remove KPR by immersing in H_2SO_4.

Except for the black wax masking these procedures were readily adapted from silicon planar technology. This unique masking technique is illustrated in the photograph of Fig. B-3 which shows a single needle mounted in the special spring fixture and held against the wax-coated slide.

(12) Clean: Use the stand procedure of No. (1).

(13) Diffusion: The diffusion parameters are typically as follows: 20 minutes at 1100°C, 40 ppm of B_2H_6 and 50 cc per minute of O_2. After the diffusion the O_2 flow is continued for approximately 5 minutes.

(14) Etch: The needles are etched in a solution of 10 parts DI H_2O and one part HF for 20 seconds.

(15) Second Oxidation: The second oxide is grown at 1100°C using a dry-wet-dry procedure as follows: 10 minutes in O_2, 30 minutes in steam, and 20 minutes in O_2.

(16) Second Mask: The second masking procedure provides for a contact window to the diffused tip of the needle. The procedure is identical to the first masking step described in No. (11) except in one important detail. It is required that the contact window be made smaller than the first or diffusion window, and lie wholly inside the diffusion window. This is accomplished by using a thinner layer of wax on the wax-coated slide. Success is dependent upon the judgement and skill of the operator. If successful, the two openings can be readily identified under a microscope.

(17) Etch: The contact window is opened by a 7 minute etch in buffered HF.

(18) Clean: This procedure is identical to the standard procedure of No. (1).

(19) Evaporate Aluminum: In the evaporation furnace the needles are masked in a special fixture so as to restrict the aluminum to a narrow strip from the tip to a point still below the beginning

of the conical portion of the needle. The objective is to provide an aluminum strip large enough for an expanded contact to the tip.

(20) Alloy: The evaporated aluminum is alloyed for 10 minutes in N_2 at 550°C.

(21) Mask: All but the upper shank of the needles are masked with apiezon black wax so as to remove the oxide from the shank prior to nickel plating.

(22) Etch: The exposed oxide on the needle shank is removed by a 30 second emersion in HF.

(23) Nickel Plate: The needle shank is nickel plated by emersion in a standard solution at 90°C for 10 minutes.

(24) Clean: This procedure is the standard procedure of No. (1).

(25) Bond Lead: A one mil gold wire is "ball" bonded to the aluminum strip.

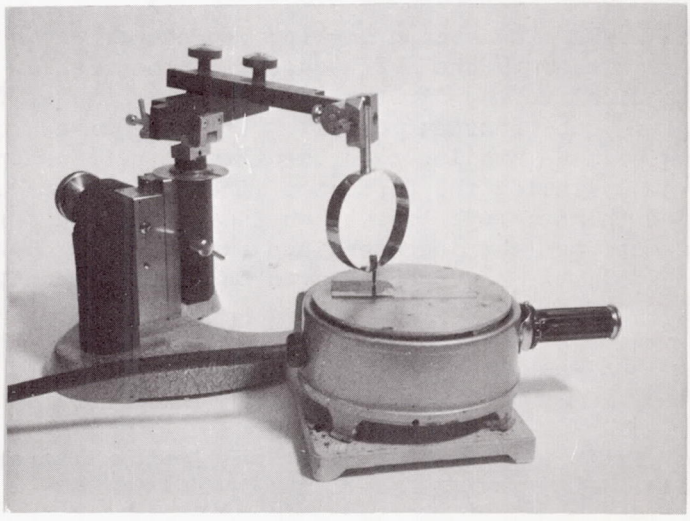

Figure B-3. A Photographic Illustration of the Black-Wax Masking Procedure

APPENDIX C

FUNDAMENTAL FREQUENCY OF A CIRCULAR DIAPHRAGM

The fundamental frequency of a clamped, circular diaphragm is given by Morse as (Ref. 11)

$$f_o = 0.934 \left(\frac{t}{2a^2}\right) \left(\frac{E}{\rho(1 - \nu^2)}\right)^{1/2} \qquad \text{(C-1)}$$

where f_o = fundamental frequency,

ρ = density,

ν = Poisson's ratio,

E = Young's Modulus,

t = diaphragm thickness, and

a = diaphragm radius.

In silicon, ν and E are direction dependent with minimum and maximum values as given below (Ref. 6):

$$0.048 < \nu < 0.403$$
$$1.3 \times 10^{12} < E < 1.88 \times 10^{12} \text{ dynes/cm}^2 . \qquad \text{(C-2)}$$

In the (111) plane, for example, ν and E are constants, i.e., $\nu = 0.358$ and $E = 1.69 \times 10^{12}$ dynes/cm^2. The density of silicon is 2.33 gm/cm^3 (Ref. 6). Using those values in Eq. (C-1), the fundamental frequency of a silicon diaphragm is given by

$$f_o = 4.26 \times 10^5 \frac{t}{a^2} , \qquad \text{(C-3)}$$

where t and a are in centimeters. For t small and a large, the fundamental frequency of a circular diaphragm achieves its lowest value. Practical values corresponding to these conditions are, for example, $t = 6.35 \times 10^{-3}$ cm. and $a = 1.27$ cm. Using these values, a low value for the fundamental frequency of a circular, silicon diaphragm is

$$f_o = 1.67 \text{ k cps} .$$

LIST OF REFERENCES

1. Research Triangle Institute, Feasibility Study of a Miniature Solid-State Pressure Transducer, by C. D. Parker, Contract No. NAS1-6249, Research Triangle Park, N. C., July 1967 (U).

2. J. J. Wortman, J. R. Hauser, and R. M. Burger, J. Appl. Phys. 35, 2122-2131, July 1964.

3. J. J. Wortman and J. R. Hauser, J. Appl. Phys. 37, 3527-3530, August 1966.

4. J. R. Hauser and J. J. Wortman, J. Appl. Phys. 37, 3884-3892, September 1966.

5. J. J. Wortman, Effect of Mechanical Strain on p-n Junctions, NASA CR-275, 1-106, August 1965.

6. J. J. Wortman, Semiconductor Piezojunction Transducers, NASA CR-1089, 1-85, June 1968.

7. Research Triangle Institute, Integrated Silicon Device Technology Volume V----Physical/Electrical Properties of Silicon, by R. A. Evans, Technical Documentary Report No. ASD-TDR-63-316, Vol. V, Contract AF 33(657)-10340, Durham, N. C., July 1965 (U) AD 605 558.

8. R. J. Roark, Formulas for Stress and Strain, 4th Ed., McGraw-Hill Book Company, New York, New York (1965).

9. J. F. Cleary, Transistor Manual, General Electric Company, Syracuse, New York, 1962.

10. W. P. Mason, Physical Acoustics and the Properties of Solids, (D. Van Nostrand Company, New York, 1958).

11. P. B. Morse, Vibration and Sound, 1st Ed., McGraw-Hill Book Company, New York, N. Y. (1936).

NASA-Langley, 1969 —— 26 CR-1366